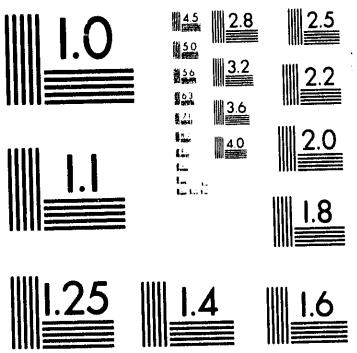
1.0
1.1
1.25
1.4
1.6
1.8
2.0
2.2
2.5
2.8
3.2
3.6
4.0
4.5
5.0

1 of 1

LA-12708-MS

Issued: December 1993

Preliminary Conceptual Model for Mineral Evolution in Yucca Mountain

C. J. Duffy

Los Alamos
NATIONAL LABORATORY
Los Alamos, New Mexico 87545

PRELIMINARY CONCEPTUAL MODEL FOR MINERAL EVOLUTION IN YUCCA MOUNTAIN

by

C. J. Duffy

ABSTRACT

I present a model for mineral alteration in Yucca Mountain, Nevada, that suggests that the mineral transformations observed there are primarily controlled by the activity of aqueous silica. The rate of these reactions is related to the rate of evolution of the metastable silica polymorphs opal-CT and cristobalite assuming that $a_{SiO_{2(aq)}}$ is fixed at the equilibrium solubility of the most soluble silica polymorph present. The rate equations accurately predict the present depths of disappearance of opal-CT and cristobalite. The rate equations have also been used to predict the extent of future mineral alteration that may result from emplacement of a high-level nuclear waste repository in Yucca Mountain. Relatively small changes in mineralogy are predicted, but I base these predictions on the assumption that emplacement of a repository would not increase the pH of water in Yucca Mountain nor increase its carbonate content. Such changes may significantly increase mineral alteration.

Some of the reactions currently occurring in Yucca Mountain consume H^+ and CO_3^{2-}. Combining reaction rate models for these reactions with water chemistry data may make it possible to estimate water flux through the basal vitrophyre of the Topopah Spring Member and to help constrain the direction and rate of flow of groundwater in Yucca Mountain.

I. INTRODUCTION

Potential detrimental effects of glass and mineral alteration may affect the suitability of Yucca Mountain in south central Nevada as a potential site for an underground high-level radioactive waste repository. This report, sponsored by the Nevada Nuclear Waste Storage Investigations (NNWSI) Project of the U.S. Department of Energy, presents a

preliminary conceptual model for mineral alteration in Yucca Mountain. I present a preliminary assessment of mineral alteration that may occur in Yucca Mountain over the lifetime of a repository. Mineral alteration will occur in Yucca Mountain because at least some of the current mineral assemblages are metastable. I am primarily concerned with the rate of transformation of these metastable mineral assemblages. The validity of performance assessment based on current rock properties is directly correlated to the persistence of current mineral assemblages. If transformation of the current mineral assemblages is unlikely over the lifetime of the repository, we can use current rock properties with confidence in performance assessment. However, possible mineral alteration could affect repository performance by changing the sorptive properties of the rock, by changing rock mechanical properties (such as strength), by changing hydraulic properties (such as permeability and porosity), or by producing or consuming water.

Mineral transformations occur in Yucca Mountain for two possible reasons. First, much of the present mineralogy is metastable because many of the minerals were formed from the low-temperature alteration of glass. The silica phases opal-CT, tridymite, and cristobalite are metastable with respect to quartz under the conditions present in Yucca Mountain. Field observations suggest that clinoptilolite and mordenite are also metastable. Because of this metastability, mineral transformations will take place in Yucca Mountain even if a repository is not built there. Second, the heating caused by a repository may induce or accelerate mineral transformations. These transformations may be caused by different mineral assemblages becoming stable or by the increased rate of transformation of metastable assemblages caused by heating. The dominant minerals in Yucca Mountain are the silica polymorphs (tridymite, opal-CT, cristobalite, and quartz), clinoptilolite, mordenite, clays, analcime, and alkali-feldspars. Lesser amounts of kaolinite and calcite are present and involved in reactions among the major phases.

The effects of heat and time are major factors that determine the present mineral distribution. The validity of the conceptual model produced by this task can therefore be at least partially assessed by how well it explains the present mineral distribution. I hypothesize that the mineral transformations in Yucca Mountain are largely controlled by the decreasing aqueous silica activity caused by the evolution of the metastable silica polymorphs to quartz. The transition of analcime plus SiO_2 to albite is the only major mineral reaction observed in Yucca Mountain that cannot plausibly be attributed to decreasing aqueous silica activity. This transformation is probably dependent on the kinetics of aluminum/silicon ordering in albite, but may also require a higher temperature

than those currently existing in Yucca Mountain. Transformation of the metastable silica polymorphs and its effects on the transformation of clays and zeolites will be my primary emphasis. I will also emphasize the rates of evolution of the metastable silica polymorphs, their relationship to the aqueous silica activity, and their effect on reactions among other minerals.

II. MINERALOGY

The mineralogy of Yucca Mountain, described in many reports on individual drill holes, is summarized by Bish and Vaniman (1985). More recent mineral abundance data have been obtained for drill holes J-13, UE-25a#1, and USW G-1 (Bish and Chipera, 1986). Electron microprobe mineral compositional data also appear in many of the individual reports. Electron microprobe data for clinoptilolite, analcime, and authigenic alkali feldspar have been collected by Broxton et al. (1986). Electron microprobe compositional analyses of mordenite are detailed by Caporuscio et al. (1982) and by Carlos (1985, 1987). Clay analyses are detailed in Caporuscio et al. (1982), Vaniman et al. (1984), and Levy (1984). The major minerals in Yucca Mountain fall into the categories of zeolites, clays, alkali feldspars, silica polymorphs, and calcite. The zeolites are primarily clinoptilolite, mordenite, and analcime. The clays are principally smectites, interlayered smectite/illite, and illite with lesser kaolinite. Tridymite, opal-CT, cristobalite, and quartz make up the silica polymorphs. Additional phases such as chlorite, laumontite, and iron, iron titanium, and manganese oxides and hydroxides are present in low abundance or very limited distribution. Biotite and hornblende are also present in limited abundance as phenocrysts.

The compositions of the major phases are variable. In order to model the chemical reactions among these phases, representative compositions have been chosen based on available microprobe analyses or accepted mineral compositions. These compositions are given in Table I. Clinoptilolite generally has Si/Al (atom ratio) between 4 and 5 (Broxton et al., 1987). The Si/Al ratios for a small group of calcium-rich clinoptilolites are between 2.8 and 3.6. The relative abundances of sodium, potassium, and calcium in Yucca Mountain clinoptilolites are highly variable. Few analyses are available for mordenite due to its generally fine grained nature and tendency to be intergrown with other minerals. However, Si/Al tends to be somewhat higher in mordenite than in clinoptilolite, generally between 5 and 6. The mordenite also appears to be enriched in sodium and depleted in potassium relative to nearby clinoptilolite. Calcium may also be somewhat depleted relative to sodium, but probably less so than potassium. Analcime is essentially a pure sodium mineral with only very minor amounts of potassium or calcium. The Si/Al ratio

of the Yucca Mountain analcimes range from 2.3 to 2.9 and show a bimodal distribution centered about approximately 2.53 and 2.75.

TABLE I

REPRESENTATIVE MINERAL COMPOSITIONS FOR YUCCA MOUNTAIN

Clinoptilolite	=	$(\frac{1}{2}Ca, Na, K)_{2.18}Al_{2.18}Si_{9.82}O_{24} \cdot nH_2O$
Mordenite	=	$(\frac{1}{2}Ca, Na, K)_{1.8}Al_{1.8}Si_{10.2}O_{24} \cdot nH_2O$
Analcime	=	$Na_{.86}Al_{.86}Si_{2.14}O_6 \cdot nH_2O$
Smectite	=	$(\frac{1}{2}Ca, Na)_{1.1}(Mg, Fe)_{.9}Al_{3.3}Si_{7.8}O_{20}(OH)_4 \cdot nH_2O$
Illite	=	$K_{1.9}(Mg, Fe)_{.9}Al_{4.1}Si_7O_{20}(OH)_4$
Kaolinite	=	$Al_4Si_4O_{10}(OH)_8$
K-feldspar	=	$KAlSi_3O_8$
Albite	=	$NaAlSi_3O_8$
Calcite	=	$CaCO_3$

The clays in Yucca Mountain are smectites, interlayered smectite/illite, and illites with small amounts of kaolinite. The smectites contain sodium, calcium, and potassium in the interlayer sites. The Al/(Mg + Fe) atom ratio varies slightly but is about 3.7. A small amount of aluminum is present in the tetrahedral sites. The illites are potassium rich with only minor calcium and sodium. The amount of iron and magnesium in the octahedral sites is about the same as in the smectite. The aluminum content of the tetrahedral sites is higher than in the smectites. The Mg/Fe ratio in both the illites and smectites is variable and appears to reflect the bulk composition of the rock. Compositional data are not available for the kaolinite from Yucca Mountain. Kaolinite has limited compositional variability (Deer et al., 1962); the ideal formula has been used.

The silica polymorphs are all essentially SiO_2. Water is generally present in the opal as are aluminum, sodium, and potassium, but they are present in minor amounts. The authigenic alkali feldspars are nearly pure albite and orthoclase endmembers, although the authigenic K-feldspars show a small amount of silicon substitution for aluminum in the ideal formula (Broxton et al., 1987). Intermediate sanidine and plagioclase phenocrysts are present as well as considerable intermediate alkali feldspar (Broxton et al., 1982) that is the product of elevated temperature devitrification during initial cooling of the tuff. Calcite analyses are not available, but this phase is probably nearly pure $CaCO_3$ with possible minor magnesium.

III. CONTROLS ON MINERAL ALTERATION

The mineralogic investigations of Yucca Mountain cited earlier reveal a consistent variation in mineralogy with depth. Unaltered glass is common in the upper part of the mountain. It is replaced by clinoptilolite and mordenite with increasing depth followed by analcime and finally albite. Smyth (1982) related these transformations to increasing temperature and suggested that in the presence of dilute waters the transition from clinoptilolite to analcime should take place at 90 to 100°C. However, data presented by Honda and Muffler (1970) and Keith et al. (1978) for drill holes in Yellowstone National Park show alternating zones of clinoptilolite and analcime in drill holes over the temperature interval from 50 to 150°C. Dibble and Tiller (1981) present an alternate model for the evolution of tuffaceous sediments in which clinoptilolite and smectite are assumed to be metastable phases that crystallize from supersaturated solutions resulting from glass dissolution. According to Dibble and Tiller (1981), a more ordered assemblage of feldspar, illite, and perhaps analcime is more stable, but is not observed initially because the more disordered smectites and zeolites crystallize more rapidly. The model of Dibble and Tiller (1981) tends to agree with the observed interlayering of clinoptilolite and analcime, but it suggests that mixtures of clinoptilolite with analcime and authigenic feldspar should be common. However, the transition zones between clinoptilolite and analcime bearing rocks are abrupt and the minerals coexist over a limited stratigraphic interval.

Kerrisk (1983) estimated thermodynamic data for clinoptilolite and mordenite and used these data in performing reaction-path calculations of groundwater chemistry and mineral formation. Kerrisk (1983) found that if quartz was allowed to precipitate, clinoptilolite and mordenite did not appear in the final mineral assemblage in any of his calculations from 25 to 175°C. However, if quartz and chalcedony precipitation was suppressed so that the aqueous silica activity could not fall below cristobalite saturation, clinoptilolite and mordenite appeared in the final assemblage at all temperatures. This is in agreement with the general conclusions of Dibble and Tiller, because only the assemblage which contains quartz can be the stable assemblage. However, it also points out that a distinction must be made between the stability of individual mineral phases and the overall assemblage.

Kerrisk's (1983) results can be better understood by observing that the general reaction of clinoptilolite to analcime is

$$\text{Na} - \text{clinoptilolite} \rightarrow \text{Analcime} + \text{m} \cdot \text{SiO}_2 + \text{n} \cdot \text{H}_2\text{O}. \quad (1)$$

Similar reactions can be written for reaction of the potassium and calcium components of clinoptilolite to K-feldspar and/or smectite. In all cases, the reactions involve the production of SiO_2. The equilibrium constant, K, for Eq. (1) can be written

$$K = \frac{a_{\text{analcime}} a^{\text{m}}_{\text{SiO}_{2(\text{aq})}} a^{\text{n}}_{\text{H}_2\text{O}}}{a_{\text{Na-clinoptilolite}}} \quad (2)$$

where a is the chemical activity. Because analcime is present as a pure sodium endmember, its activity is 1 as is the activity of H_2O for the dilute groundwaters of Yucca Mountain. To a first approximation, the activity of Na-clinoptilolite is the mole fraction, x, of the sodium endmember present in the clinoptilolite. Equation (2) therefore reduces to

$$K = \frac{a^{\text{m}}_{\text{SiO}_{2(\text{aq})}}}{x_{\text{Na-clinoptilolite}}}. \quad (3)$$

Equation (3) demonstrates that at a given temperature and clinoptilolite composition an aqueous silica activity exists at which the clinoptilolite and analcime are in equilibrium. Above that value, clinoptilolite is stable; below that value analcime is stable. Kerrisk's (1983) calculations suggest that the equilibrium value is between cristobalite and chalcedony saturation. I wish to stress that, although the assemblage of cristobalite, or opal-CT, and clinoptilolite is probably metastable as suggested by Dibbie and Tiller (1981), if the aqueous silica activity is high, the clinoptilolite may be stable even though the total assemblage is not. If the aqueous silica activity is high, minerals that are part of the most stable assemblage could react to form clinoptilolite.

IV. AQUEOUS SILICA ACTIVITY

The forms of solid SiO_2 are regulating factors controlling the aqueous silica. Fig. 1 shows the solubility of various forms of SiO_2 based on the analysis of Walther and Helgeson (1977), and presents water composition data from Yucca Mountain and vicinity (Kerrisk, 1987). The "beta-cristobalite" in Walther and Helgeson (1977) is almost certainly a highly disordered opal-CT (Murata and Larson, 1975). Opal-CT has varying degrees of stacking disorder. It varies continuously from highly disordered opal-CT to well-ordered cristobalite. I therefore assume that the solubility of opal-CT varies between that of "beta-cristobalite"

and cristobalite. If an opal-CT is more disordered than "beta-cristobalite," the solubility that opal-CT is probably slightly higher than "beta-cristobalite". Most of the waters fall within the range of opal-CT saturation. Some of the analyses above "beta-cristobalite" saturation may represent the effects of glass dissolution, but most are probably within the model and analytical uncertainties involved. Fig. 2 shows aqueous silica analyses of waters from Yucca Mountain and the immediate vicinity. All of the waters fall within the opal-CT saturation field, with the exception of the high-temperature sample from UE-25b#1. Most of the interval that this sample from UE-25b#1 comes is probably at sufficient depth that quartz is the only form of SiO_2 present.

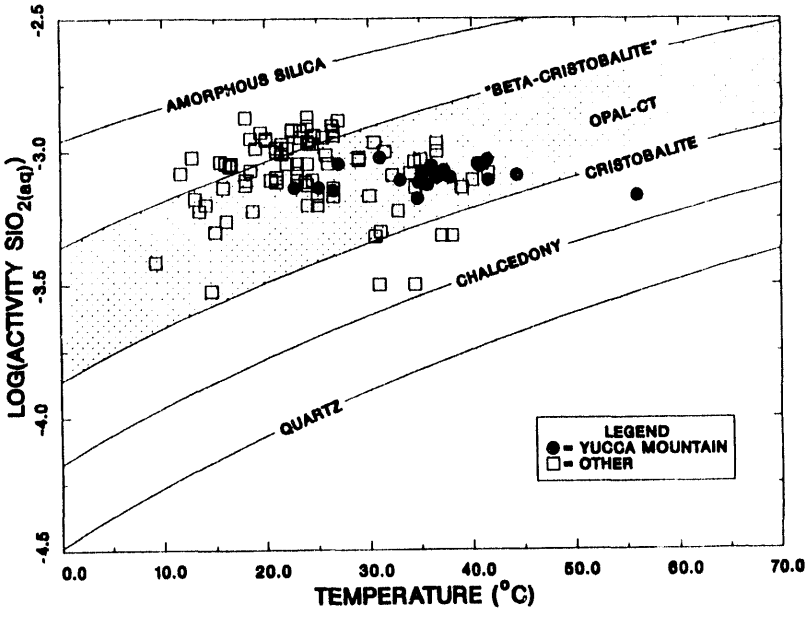

Fig. 1. Aqueous silica content of waters from Yucca Mountain and vicinity. Waters labeled "Other" are not from Yucca Mountain, but are from the general area (Kerrisk, 1987). Shaded area represents the probable range of opal-CT solubility.

Most of the water samples were obtained by pumping the entire well so that the measured temperatures and silica concentrations are composite numbers weighted in favor of zones of high flow. Fig. 3 shows temperatures and silica concentrations from packed-off zones within wells. Although silica solubility generally increases with increasing temperature for a given mineral, the deeper, hotter samples from these wells show consistently lower dissolved silica than do the cooler samples taken higher in the well. The more soluble silica polymorphs present at shallower depths are replaced by quartz at greater depth.

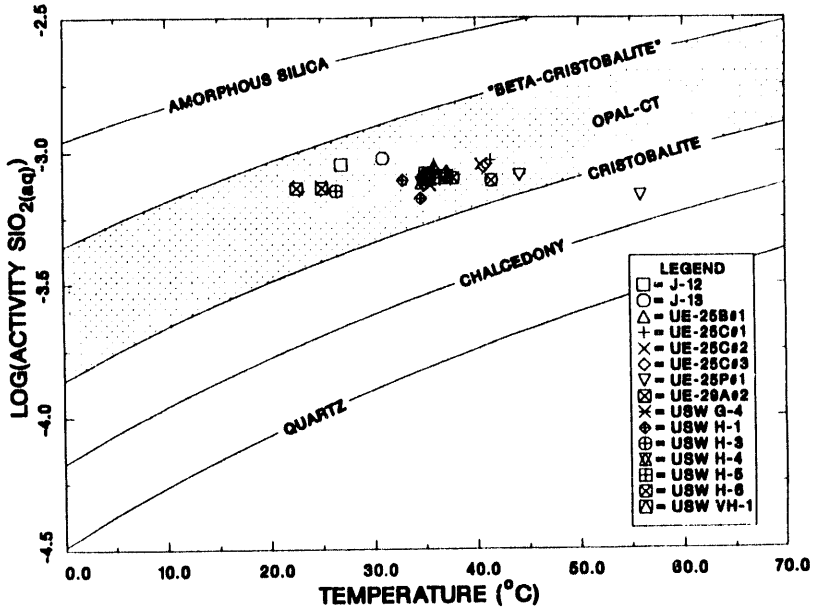

Fig. 2. Aqueous silica content of waters from Yucca Mountain and immediate vicinity.

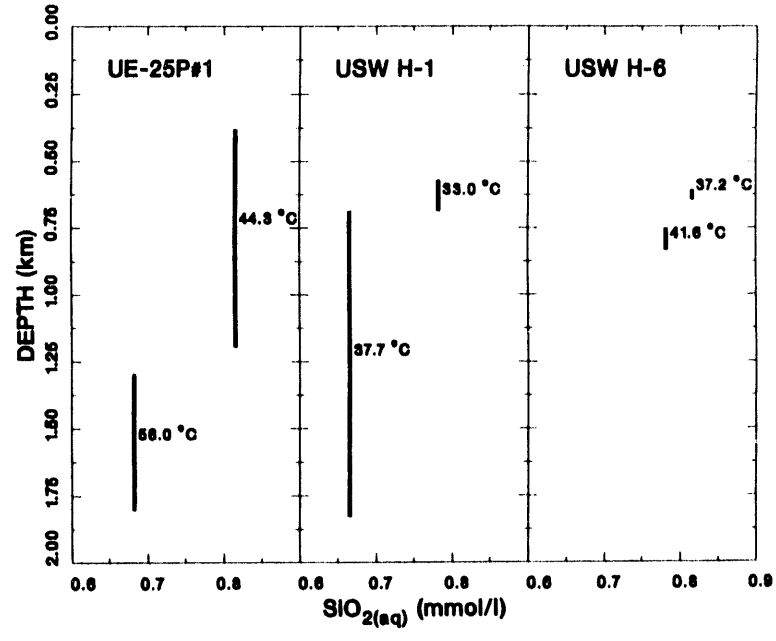

Fig. 3. Aqueous silica content and temperature of water from packed-off zones in drill holes in Yucca Mountain. Vertical bars represent the packed-off interval from which the water sample was taken.

These observations suggest that the distribution of silica polymorphs controls aqueous silica activity in Yucca Mountain. Other reactions, such as the conversion of clinoptilolite to analcime, may also influence the aqueous silica activity, but this influence will be confined to the range of silica activity where the reaction is taking place.

I assume that the aqueous silica activity is controlled at the solubility of the most soluble silica polymorph present (Duffy, 1993). The high degree of correlation between the occurrence of clinoptilolite and presence of quartz and/or opal-CT or cristobalite (Honda and Muffler, 1970; Moiola, 1970; Keith et al., 1978; Bish and Chipera, 1986) can be explained by stabilization of the clinoptilolite by the high aqueous silica activity produced by the metastable silica phases. Lower aqueous silica activity produced by equilibration with quartz accounts for the appearance of analcime with quartz only.

V. MINERAL ALTERATION IN YUCCA MOUNTAIN

The transformation of clinoptilolite must produce phases in addition to analcime because only the sodium component of the clinoptilolite can be incorporated into the analcime. These additional reactions will be of the form

$$\mathrm{K-clinoptilolite} \rightarrow \mathrm{K-product_1} + \mathrm{m}\cdot\mathrm{SiO_2} + \mathrm{n}\cdot\mathrm{H_2O}, \tag{4}$$

$$\mathrm{Na-clinoptilolite} \rightarrow \mathrm{Na-product_2} + \mathrm{m}\cdot\mathrm{SiO_2} + \mathrm{n}\cdot\mathrm{H_2O}, \tag{5}$$

and

$$\mathrm{Ca-clinoptilolite} \rightarrow \mathrm{Ca-product_3} + \mathrm{m}\cdot\mathrm{SiO_2} + \mathrm{n}\cdot\mathrm{H_2O}. \tag{6}$$

I will assume, for the moment, that these reactions produce positive amounts of silica. Thus decreasing aqueous silica activity will lead to a decrease in the clinoptilolite and only one product will be produced in addition to SiO_2 and H_2O. The equilibrium constants for Eqs. (4), (5), and (6) are

$$K = \frac{a^{\mathrm{m}}_{\mathrm{SiO_{2(aq)}}}\, a_{\mathrm{K-product_1}}}{a_{\mathrm{K-clinoptilolite}}} \tag{7}$$

$$K = \frac{a^{m}_{SiO_{2(aq)}} x_{Na-product_2}}{x_{Na-clinoptilolite}} \tag{8}$$

$$K = \frac{a^{m}_{SiO_{2(aq)}} x_{Ca-product_3}}{x_{Ca-clinoptilolite}} \tag{9}$$

respectively, where $K - product_1$, $Na - product_2$, and $Ca - product_3$ are the potassium, sodium, and calcium endmembers of $product_1$, $product_2$, and $product_3$.

For a constant $x_{product}$ the equilibrium value of $x_{clinoptilolite}$ will decrease with decreasing $a_{SiO_{2(aq)}}$. The clinoptilolite will begin to be depleted and the product phase will begin to form when the equilibrium mole fraction of the endmember clinoptilolite (Na-clinoptilolite in the case of the reaction to analcime) drops below the mole fraction present in the clinoptilolite, if the product is a pure sodium, calcium, or potassium phase such as analcime. If the product phase has a variable sodium, calcium, and potassium content, as is the case with smectite, the product is stable when

$$\sum_i x_i = 1, \tag{10}$$

where the sum is over all components in the product. Equation (10) also applies to the sum of the mole fractions of the components of stable clinoptilolite.

The clinoptilolite's original composition depends on the minerals with which it is in equilibrium at high $a_{SiO_{2(aq)}}$ such as mordenite, and perhaps, alkali feldspar and on the bulk composition of the rock. As $a_{SiO_{2(aq)}}$ decreases, the x_i for the product phase will increase (as determined by Eqs. (7), (8), and (9)), but no product will be formed until Eq. (10) is satisfied. When Eq. (10) is satisfied, the reaction of clinoptilolite to form product will progress with decreasing $a_{SiO_{2(aq)}}$. As this reaction proceeds, the clinoptilolite will be depleted in the components with higher x_i in the product than in the clinoptilolite and will be enriched in components with lower x_i. This reaction will continue until the sum of the x_i for clinoptilolite falls below 1, at which point the remainder of the clinoptilolite will react to form product.

Figs. 4-9 show the mole % of calcium, potassium, and sodium relative to the sum of calcium, potassium, plus sodium for clinoptilolite from drill holes in Yucca Mountain (Broxton et al. 1986) as a function of depth. Figs. 4-9 also show available whole rock

analyses. Clinoptilolite composition shows clear variations that are not associated with variations in the bulk composition of the rock. Figs. 10-15 show the same clinoptilolite compositional data as Figs. 4-9 plus clinoptilolite, mordenite, glass, and silica polymorph abundance data determined by x-ray diffraction. Mineral abundance data for USW G-1 and J-13 are derived from Bish and Chipera (1986), USW G-2 data are derived from Caporuscio et al. (1982), and USW G-3 and USW G-4 data are derived from Bish and Vaniman (1985). The data shown for UE-25a#1-25b#1h are for UE-25a#1 from Bish and Chipera (1986) from 26.6 to 759.6 m and for UE-25b#1h from Caporuscio et al. (1982) from 769.6 to 1215.5 m. The designation UE-25a#1-25b#1h is used for the combined data from these two drill holes because they are closely associated laterally, but mineralogic data are available from only a portion of each drill hole.

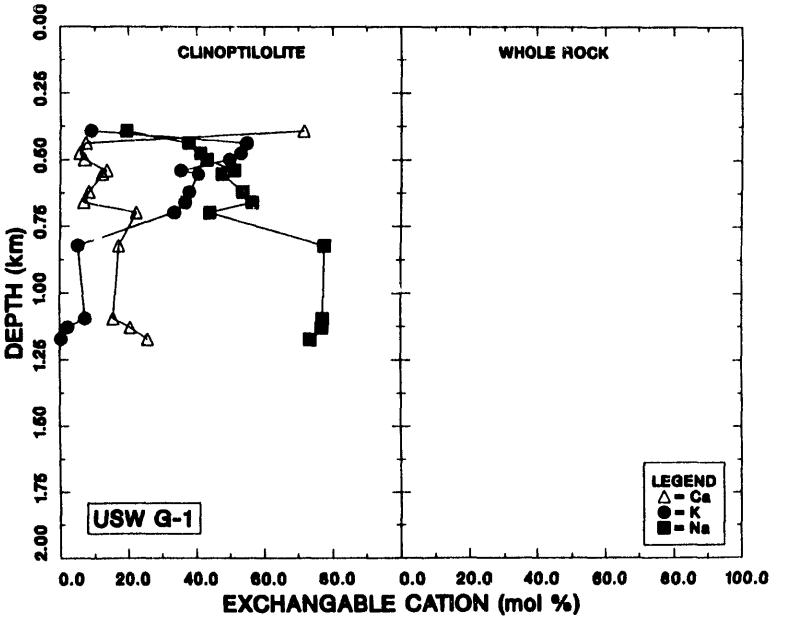

Fig. 4. Percentage of sodium, potassium, and calcium in clinoptilolite from USW G-1 relative to total sodium + potassium + calcium. No whole rock data were available for USW G-1.

Figs. 10-15 show the clear correlation between the presence of opal-CT and/or cristobalite and clinoptilolite. Clinoptilolite tends to extend to slightly greater depth than cristobalite, but in reduced abundance. Clinoptilolite, however, tends not to coexist with cristobalite and tridymite in the upper part of Yucca Mountain. Opal-CT is not shown in USW G-2, USW G-3, and USW G-4 because the distinction was not made between cristobalite and opal-CT when these analyses were made. In USW G-1, UE-25a#1, and J-13,

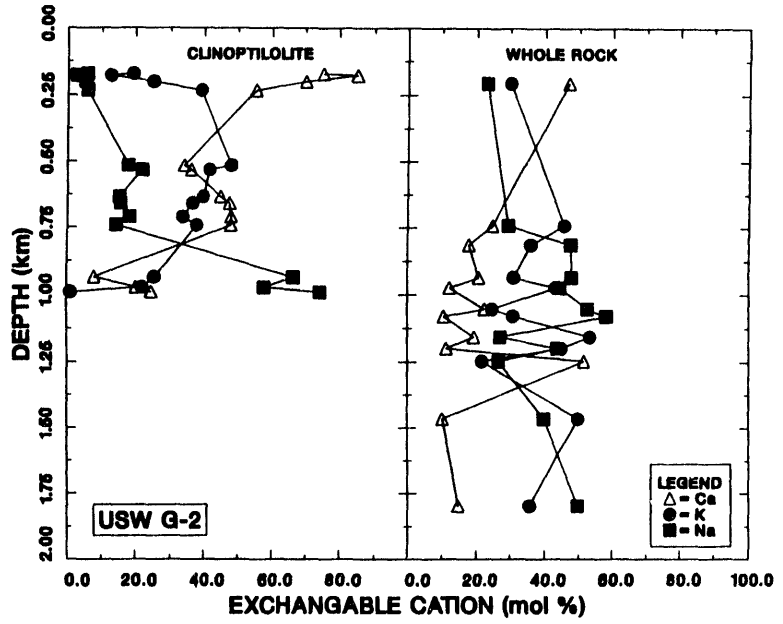

Fig. 5. Percentage of sodium, potassium, and calcium in clinoptilolite and whole rock from USW G-2 relative to total sodium + potassium + calcium.

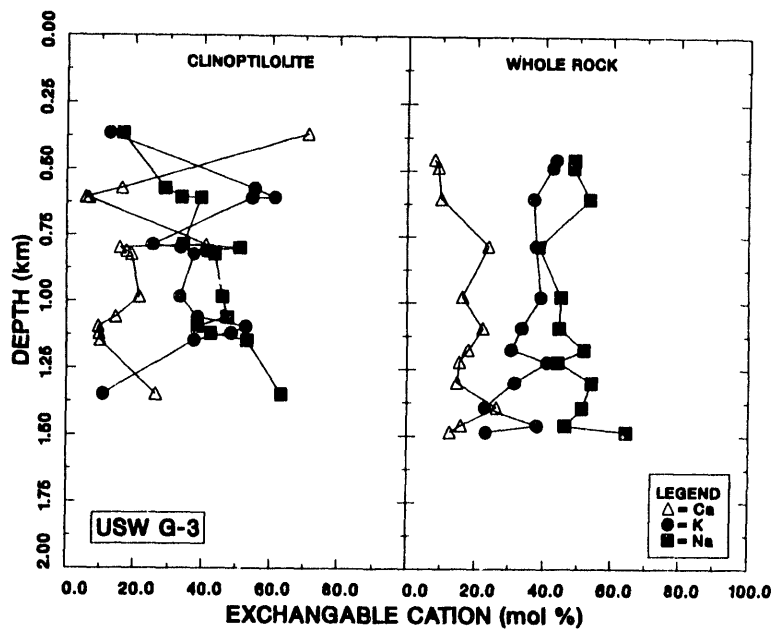

Fig. 6. Percentage of sodium, potassium, and calcium in clinoptilolite and whole rock from USW G-3 relative to total sodium + potassium + calcium.

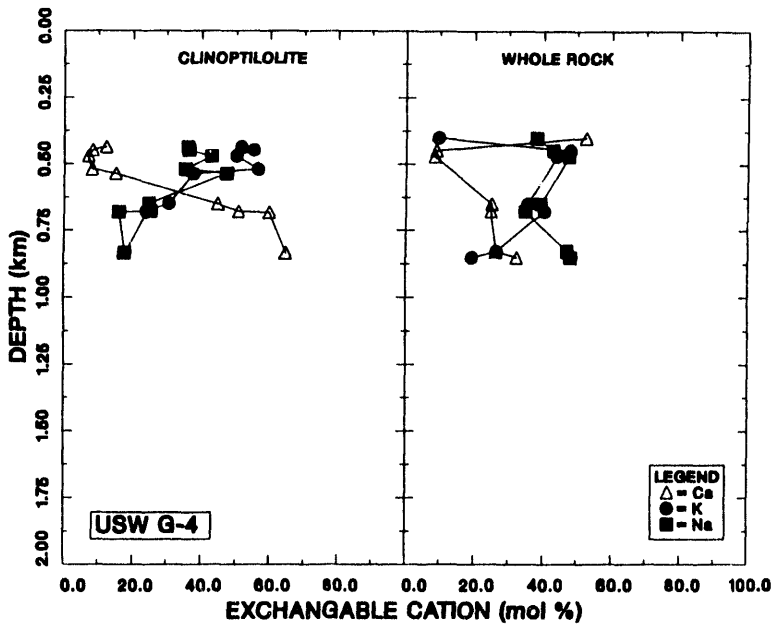

Fig. 7. Percentage of sodium, potassium, and calcium in clinoptilolite and whole rock from USW G-4 relative to total sodium + potassium + calcium.

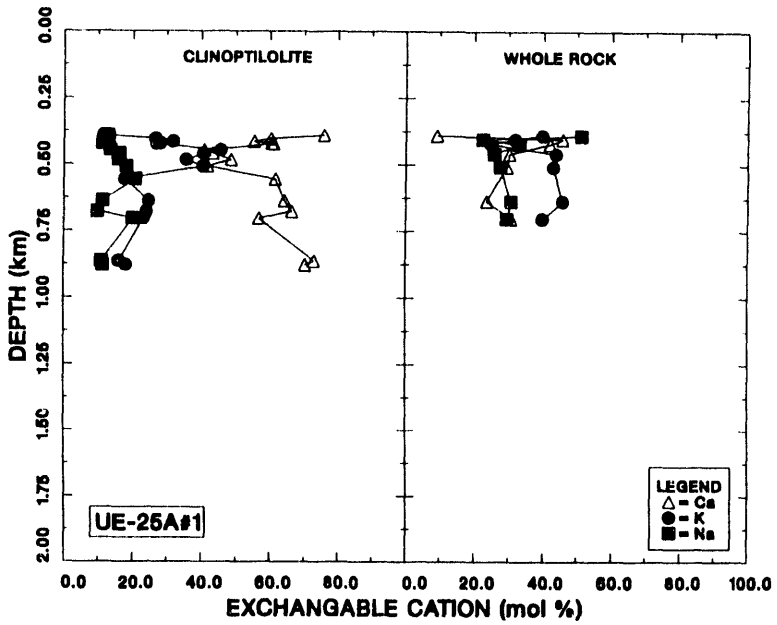

Fig. 8. Percentage of sodium, potassium, and calcium in clinoptilolite and whole rock from UE-25a#1 relative to total sodium + potassium + calcium.

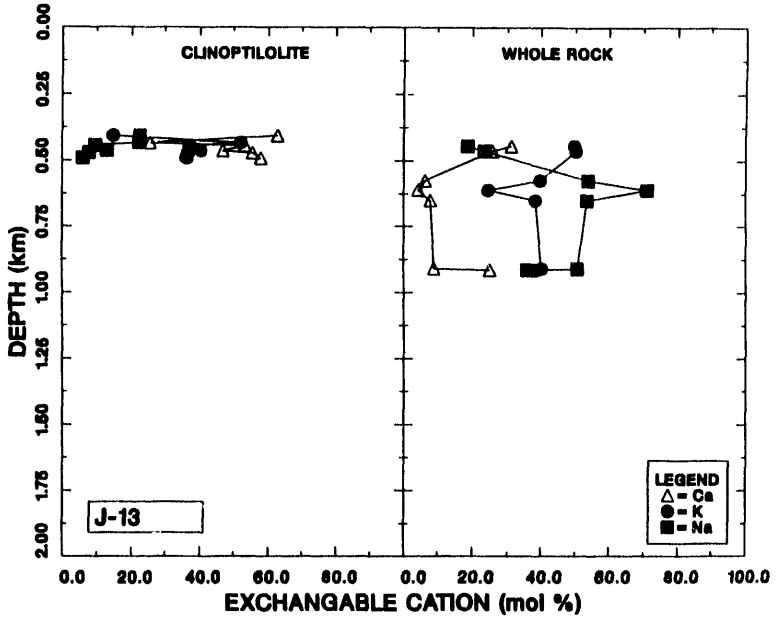

Fig. 9. Percentage of sodium, potassium, and calcium in clinoptilolite and whole rock from J-13 relative to total sodium + potassium + calcium.

where opal-CT was distinguished from cristobalite, an excellent correlation exists between high abundance of clinoptilolite and the presence of opal-CT. Mordenite and clinoptilolite tend to occur together. The sodium-potassium-calcium contents of the clinoptilolite tend to show calcium enrichment at the top of the sequence followed at increasing depth by a zone of relatively constant composition that generally follows the bulk composition of the whole rock. At greater depth, the clinoptilolite becomes depleted in potassium.

Figs. 16-21 are compiled from the same sources as are Figs. 10-15 and show the clinoptilolite sodium-potassium-calcium contents along with the mineralogic composition of the rocks. Glass, tridymite, and mica have not been included in these diagrams because they do not appear to be involved in the reactions that will be discussed. Their inclusion would only further complicate the figures. Fig. 16 of USW G-1 and Fig. 20 of UE-25a#1-25b#1h suggest that potassium depletion in the clinoptilolite is closely associated with the disappearance of opal-CT and begins before appreciable smectite crystallization. The alkali feldspar content of the rocks containing potassium-poor clinoptilolite is higher than those containing more potassium-rich clinoptilolite. Potassium depletion of the clinoptilolite is, therefore, probably due to the reaction

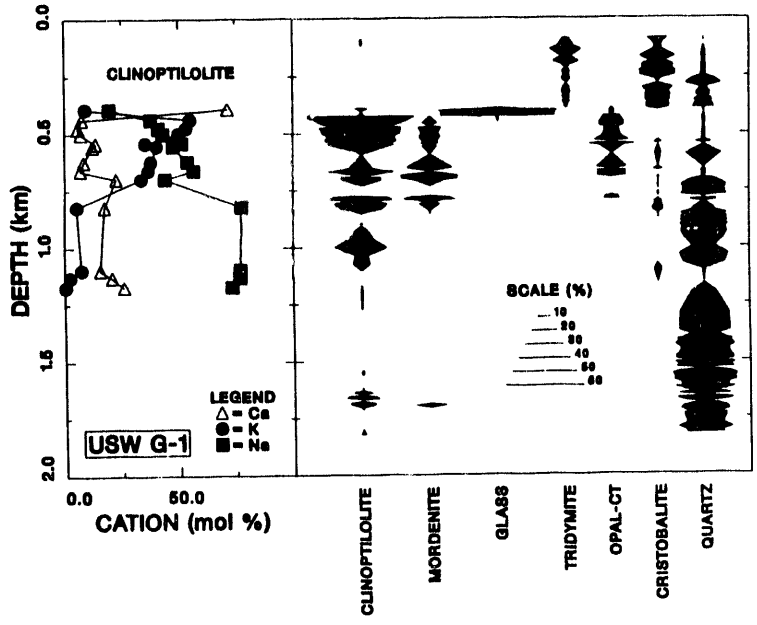

Fig. 10. Sodium, potassium, and calcium content of clinoptilolite and weight percentages of clinoptilolite, mordenite, glass and silica polymorphs in USW G-1.

$$\underset{\text{K-clinoptilolite}}{K_{2.18}Al_{2.18}Si_{9.82}O_{24}} \rightarrow 2.18\underset{\text{K-feldspar}}{KAlSi_3O_8} + 3.28\underset{\text{aqueous silica}}{SiO_2}. \tag{11}$$

The water of hydration has not been included in this reaction or those that follow because of the lack of knowledge of the hydration state of the minerals containing water of hydration. Water is present throughout Yucca Mountain, so the availability of water should not limit the reactions. The activity of water will not be important in the equilibrium constants so long as the water is dilute. At the low temperatures of concern in Yucca Mountain, K-feldspar is essentially a pure phase so the equilibrium constant for Eq. (11) is given by

$$K = \frac{a^{3.28}_{SiO_{2(aq)}}}{x_{K-clinoptilolite}}. \tag{12}$$

Fig. 22 shows the equilibrium mole fraction of K-clinoptilolite coexisting with K-feldspar assuming that the equilibrium $x_{K-clinoptilolite}$ at cristobalite saturation is 0.06. The diagram is calculated at 28°C, but the relationship between the equilibrium $x_{K-clinoptilolite}$ and the solubilities of the various silica polymorphs probably remains nearly constant over temperatures of importance in Yucca Mountain. Only the values of $a_{SiO_{2(aq)}}$ would change with the temperature. The $x_{K-clinoptilolite}$ values predicted by Fig. 22 are

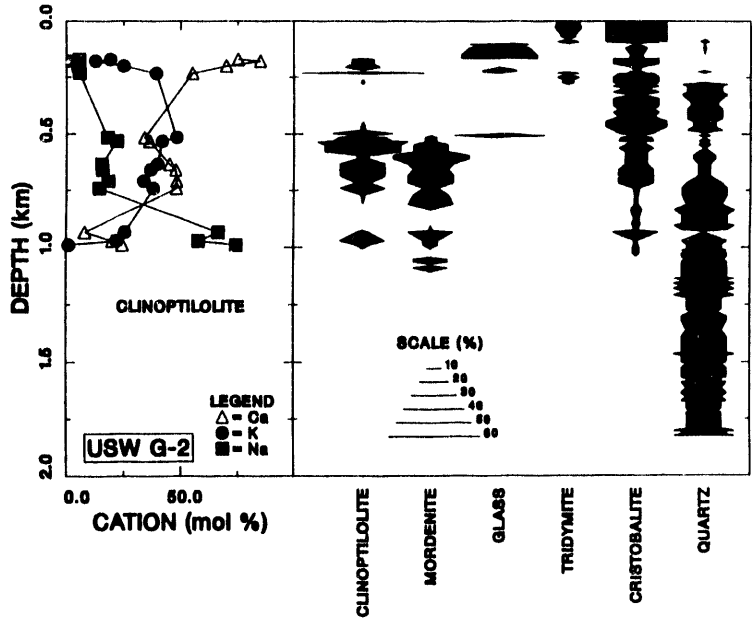

Fig. 11. Sodium, potassium, and calcium content of clinoptilolite and weight percentages of clinoptilolite, mordenite, glass and silica polymorphs in USW G-2.

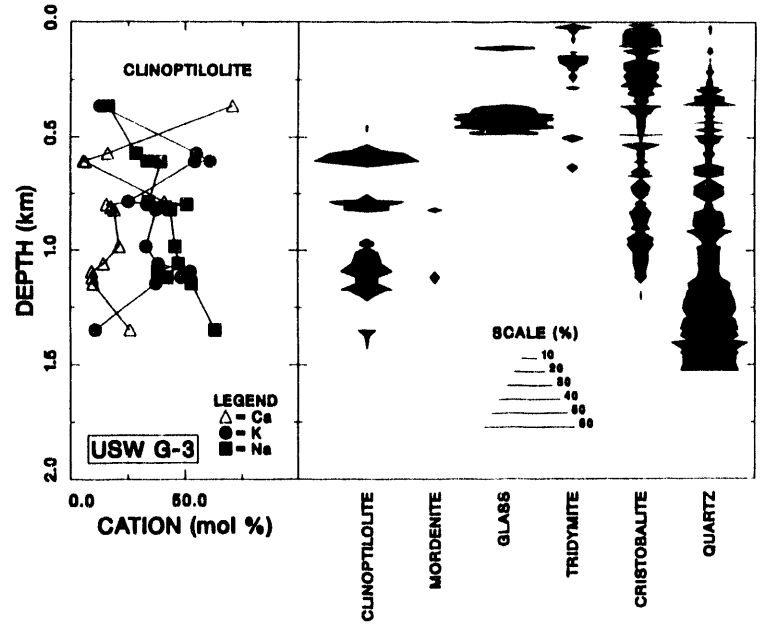

Fig. 12. Sodium, potassium, and calcium content of clinoptilolite and weight percentages of clinoptilolite, mordenite, glass and silica polymorphs in USW G-3.

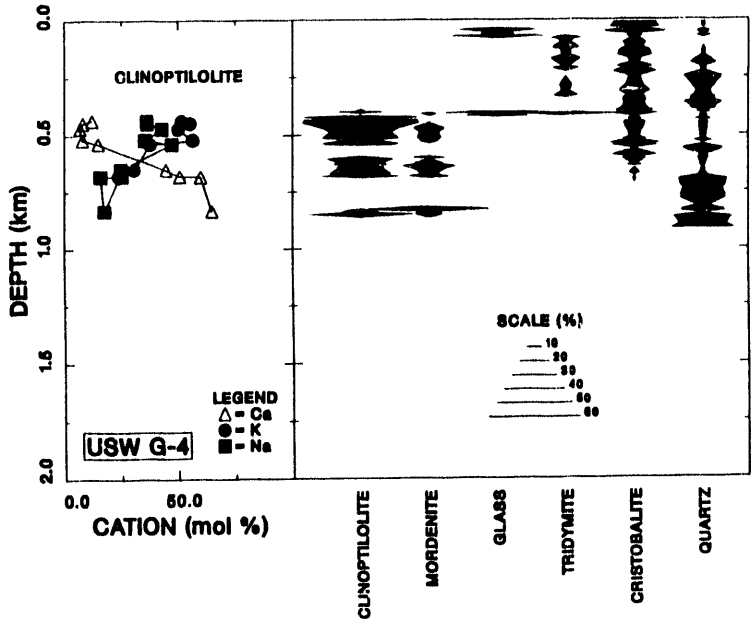

Fig. 13. Sodium, potassium, and calcium content of clinoptilolite and weight percentages of clinoptilolite, mordenite, glass and silica polymorphs in USW G-4.

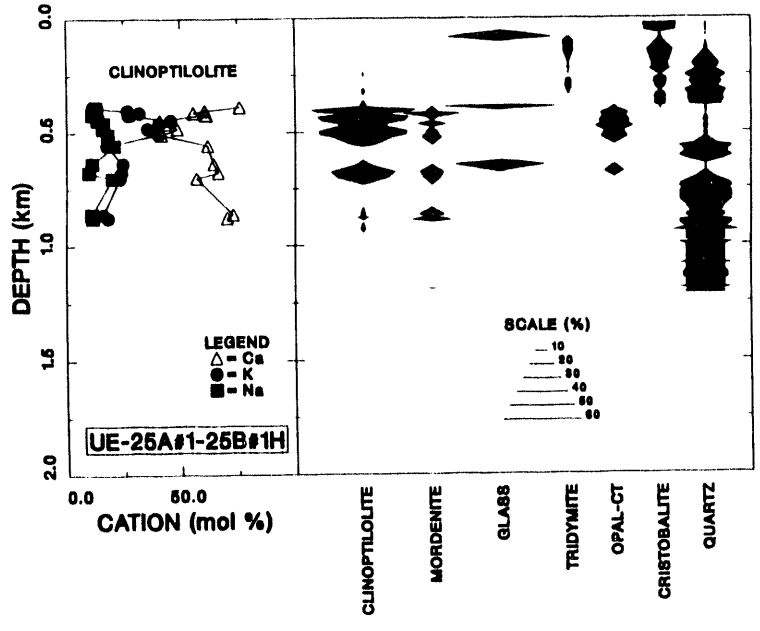

Fig. 14. Sodium, potassium, and calcium content of clinoptilolite and weight percentages of clinoptilolite, mordenite, glass and silica polymorphs in UE-25a#1 and UE-25b#1h.

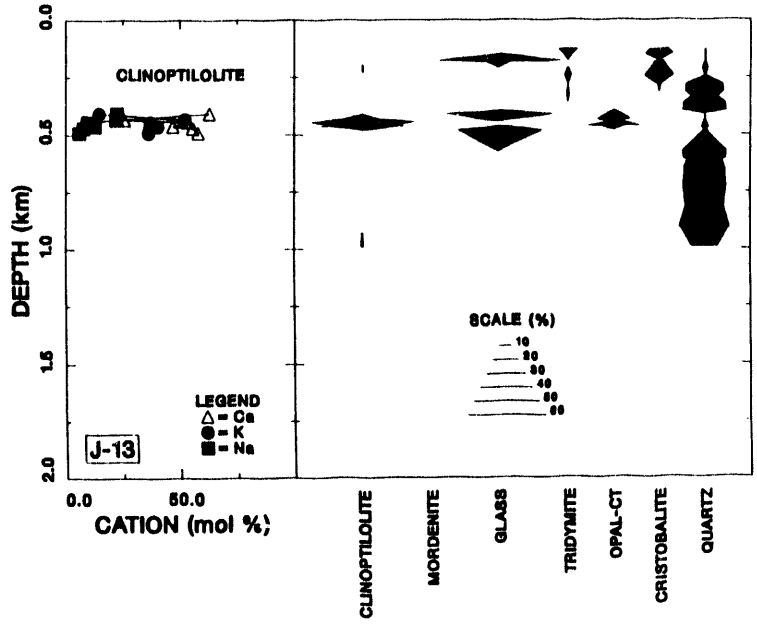

Fig. 15. Sodium, potassium, and calcium content of clinoptilolite and weight percentages of clinoptilolite, mordenite, glass and silica polymorphs in J-13.

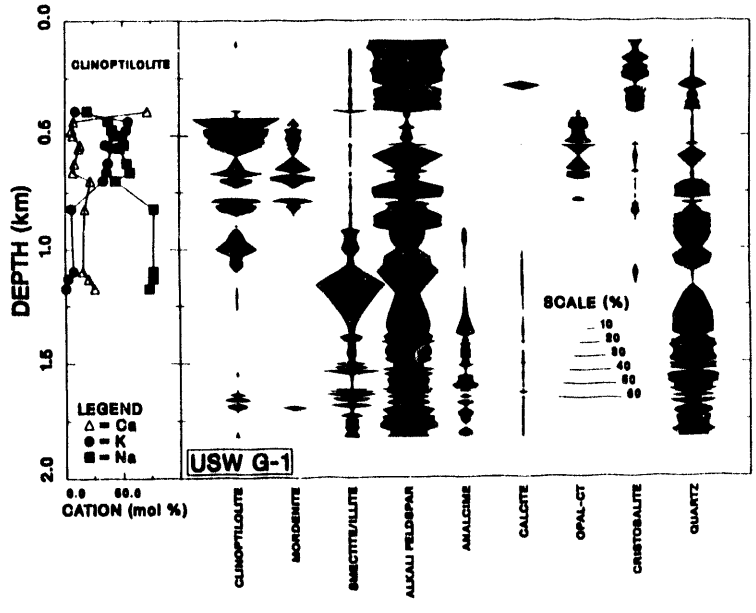

Fig. 16. Sodium, potassium, and calcium content of clinoptilolite and weight percentages of minerals in USW G-1.

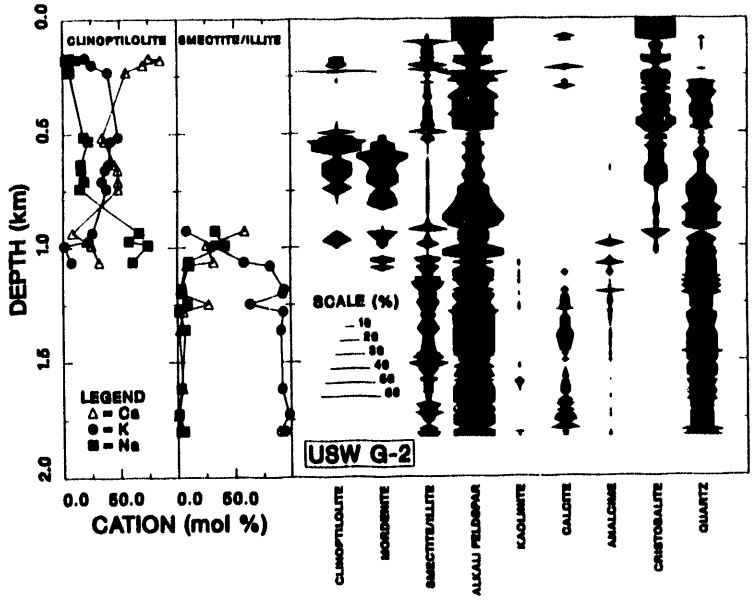

Fig. 17. Sodium, potassium, and calcium content of clinoptilolite and clay and weight percentages of minerals in USW G-2.

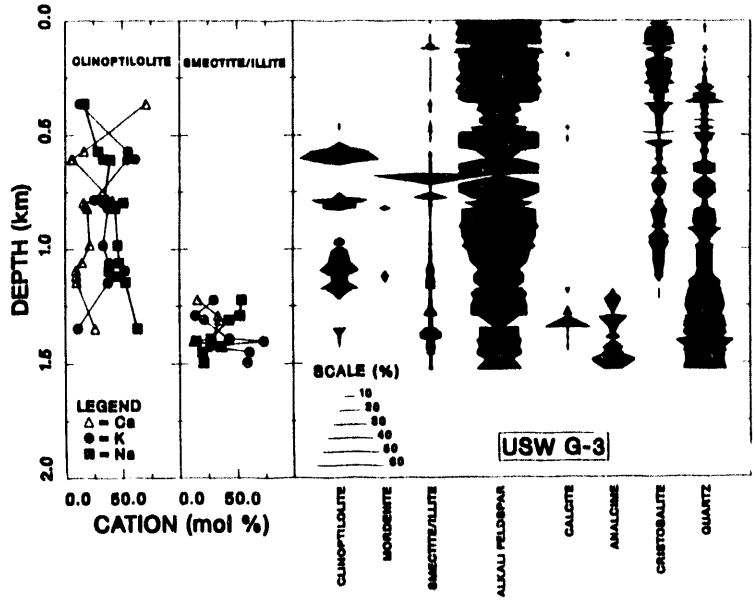

Fig. 18. Sodium, potassium, and calcium content of clinoptilolite and clay and weight percentages of minerals in USW G-3.

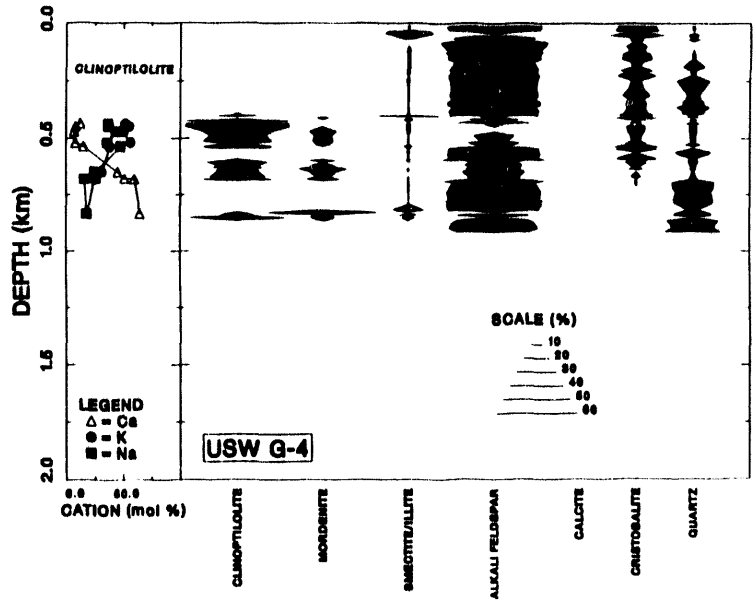

Fig. 19. Sodium, potassium, and calcium content of clinoptilolite and weight percentages of minerals in USW G-4.

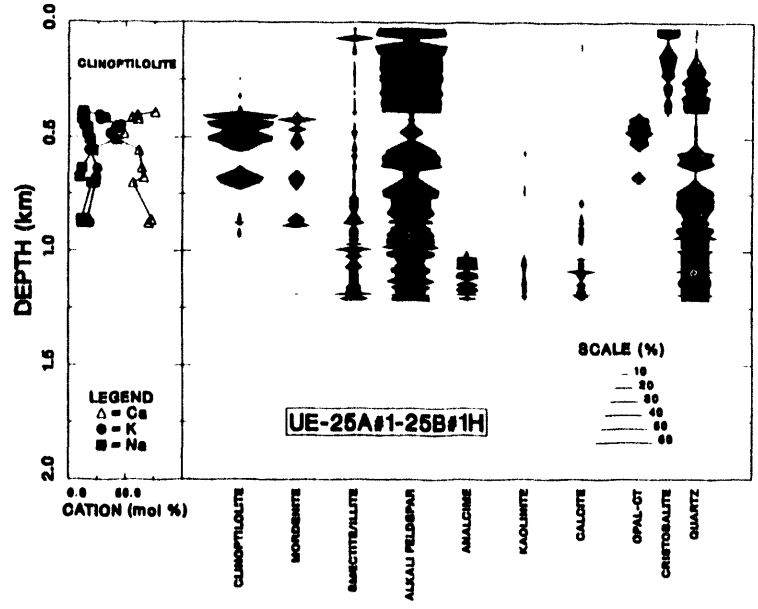

Fig. 20. Sodium, potassium, and calcium content of clinoptilolite and weight percentages of minerals in UE-25a#1 and UE-25b#1h.

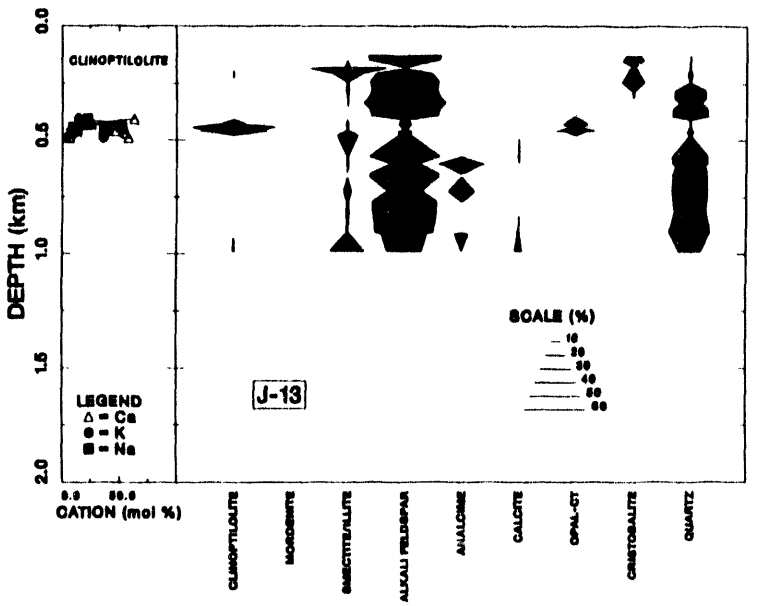

Fig. 21. Sodium, potassium, and calcium content of clinoptilolite and weight percentages of minerals in J-13.

consistent with the assumption that $a_{SiO_{2(aq)}}$ is fixed at the solubility of the most soluble silica polymorph present, except perhaps in USW G-1 where only quartz is present with the clinoptilolite. In USW G-1, $a_{SiO_{2(aq)}}$ may be controlled by reaction among the clays and zeolites. Where clinoptilolite coexists with opal-CT, the potassium content of the clinoptilolite gradually decreases with increasing depth. The kinetic model of the silica polymorph transitions (to be presented later in detail) suggests that the depth distribution of silica polymorphs results from their temperature history with the nonwelded tuff in the upper part of the mountain experiencing nearly constant temperature near the present value. Fig. 23 presents the results for a model with a constant temperature of 28°C. The 28°C temperature of the model duplicates the current temperature at about 450 m in USW G-1 (Sass and Lachenbruch, 1982) in the upper part of the Tuff of Calico Hills. The age of Calico Hills tuff is about 13.4 m.y. (Marvin et al., 1970). The model predicts that the opal-CT at this depth of 450 m would have an 101 spacing about two-thirds of the way between highly disordered opal-CT and cristobalite. Although the relationship between 101 spacing and solubility is not known, the solubility of such an opal-CT is probably roughly midway between that of "beta-cristobalite" and cristobalite, which would be in equilibrium with K-feldspar and clinoptilolite with $x_{K-clinoptilolite}$ of about 0.5, in reasonable agreement with the observed value of 0.58.

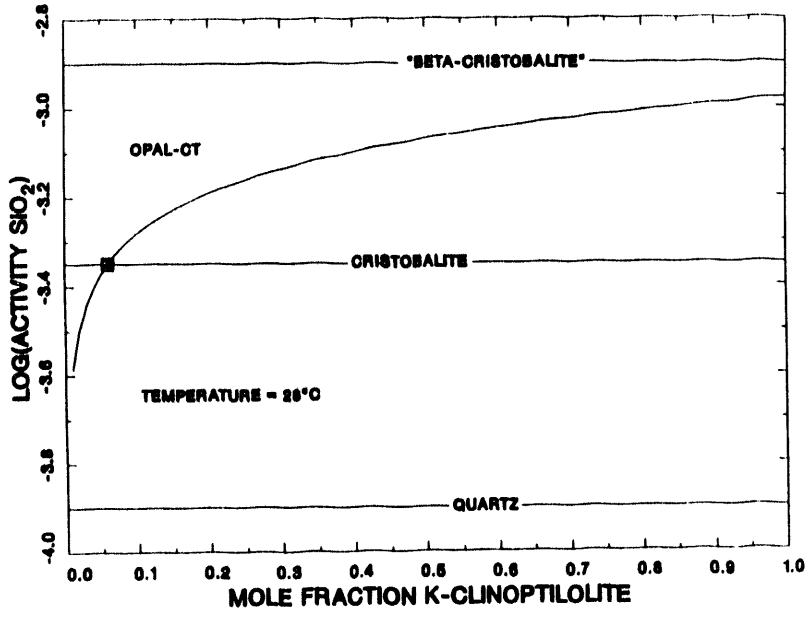

Fig. 22. Equilibrium $x_{\mathrm{K-clinoptilolite}}$ vs. $a_{\mathrm{SiO}_{2(\mathrm{aq})}}$ for Eq. (11).

In USW G-1 and USW G-2, analcime begins to form when $x_{\mathrm{Na-clinoptilolite}}$ rises to about 0.77. The equation for this reaction is

$$\underset{\text{Na-clinoptilolite}}{\mathrm{Na_{2.18}Al_{2.18}Si_{9.82}O_{24}}} \rightarrow 2.53\underset{\text{analcime}}{\mathrm{Na_{.86}Al_{.86}Si_{2.14}O_6}} + 4.41\underset{\text{aqueous silica}}{\mathrm{SiO_2}}. \tag{13}$$

Because analcime is a pure sodium phase,

$$K = \frac{a^{4.41}_{\mathrm{SiO}_{2(\mathrm{aq})}}}{x_{\mathrm{Na-clinoptilolite}}}. \tag{14}$$

Fig. 24 shows the relationship between $a_{\mathrm{SiO}_{2(\mathrm{aq})}}$ and $x_{\mathrm{Na-clinoptilolite}}$ in equilibrium with analcime based on Eq. (14) with the assumption that the equilibrium $x_{\mathrm{Na-clinoptilolite}}$ at cristobalite saturation is 0.77. The clinoptilolite compositional data for USW G-3 suggest that $a_{\mathrm{SiO}_{2(\mathrm{aq})}}$ is appreciably above cristobalite saturation, based on $x_{\mathrm{K-clinoptilolite}}$, until cristobalite/opal-CT disappears from the hole. Below the disappearance of cristobalite, $x_{\mathrm{Na-clinoptilolite}}$ suggests that $a_{\mathrm{SiO}_{2(\mathrm{aq})}}$ is slightly below cristobalite saturation, in agreement with the observed mineralogy, while $x_{\mathrm{K-clinoptilolite}}$ suggests that $a_{\mathrm{SiO}_{2(\mathrm{aq})}}$ is slightly above cristobalite saturation. In USW G-4, UE-25a#1-25b#1h, and J-13, clinoptilolite does

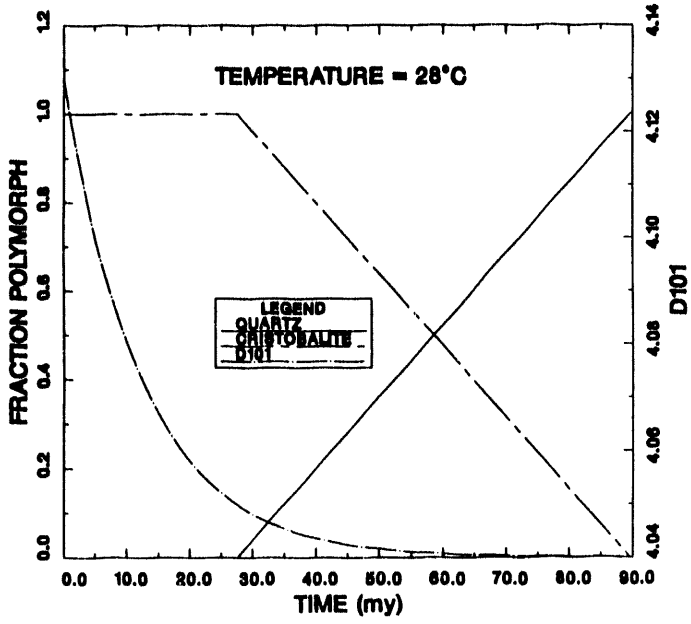

Fig. 23. Model prediction for the evolution of silica polymorphs at 28°C. D101 is the spacing of the 101 planes in the crystal lattice of opal-CT.

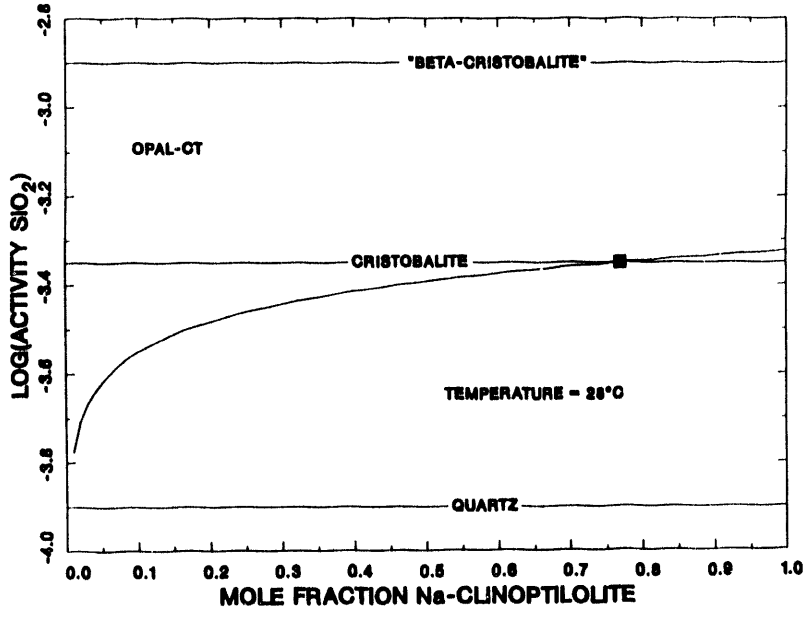

Fig. 24. Equilibrium $x_{\text{Na-clinoptilolite}}$ vs. $a_{SiO_{2(aq)}}$ for Eq. (13).

not coexist with analcime due to the low sodium content of the clinoptilolite. In these holes, the remaining clinoptilolite apparently transforms to smectite before sufficiently low $a_{SiO_{2(aq)}}$ is reached for reaction to analcime.

The reaction of clinoptilolite to smectite can be described by the reactions

$$\underset{\text{Ca-clinoptilolite}}{Ca_{1.09}Al_{2.18}Si_{9.82}O_{24}} + .59(Mg,Fe)O + 1.46H^+ + 0.73CO_3^{2-}$$

$$\rightarrow \underset{\text{Ca-smectite}}{0.66Ca_{.55}(Mg,Fe)_{.9}Al_{3.3}Si_{7.8}O_{20}(OH)_4} + \underset{\text{calcite}}{0.73CaCO_3} + \underset{\text{aqueous silica}}{4.67SiO_2} \tag{15}$$

and

$$\underset{\text{Na-clinoptilolite}}{Na_{2.18}Al_{2.18}Si_{9.82}O_{24}} + 1.98\underset{\text{Ca-smectite}}{Ca_{.55}(Mg,Fe)_{.9}Al_{3.3}Si_{7.8}O_{20}(OH)_4}$$

$$\rightarrow \underset{\text{Ca-clinoptilolite}}{Ca_{1.09}Al_{2.18}Si_{9.82}O_{24}} + 1.98\underset{\text{Na-smectite}}{Na_{1.1}(Mg,Fe)_{.9}Al_{3.3}Si_{7.8}O_{20}(OH)_4} \tag{16}$$

with equilibrium constants

$$K = \frac{a_{SiO_{2(aq)}}^{4.67} x_{Ca-smectite}^{.66}}{a_{H^+}^{1.46} a_{CO_3^{2-}}^{.73} x_{Ca-clinoptilolite}} \tag{17}$$

and

$$K = \frac{x_{Ca-clinoptilolite} x_{Na-smectite}^{1.98}}{x_{Na-clinoptilolite} x_{Ca-smectite}^{1.98}}. \tag{18}$$

An equation similar to Eq. (17) could be written to describe exchange of potassium and calcium between clinoptilolite and smectite, but little potassium remains in the clinoptilolite when the transformation to smectite occurs.

Equation (17) shows that the transformation of clinoptilolite to smectite is highly dependent on $a_{SiO_{2(aq)}}$, but is also dependent on the pH and $a_{CO_3^{2-}}$. The progress of

Eq. (15) is limited by the supply of CO_3^{2-}. As the reaction proceeds, $a_{CO_3^{2-}}$ will fall until the reaction stops unless additional CO_3^{2-} is brought into the rock by moving water. The supply of iron and magnesium could also limit this reaction. Although small amounts of iron and magnesium are found in the clinoptilolite, they are sufficient for the formation of only very small amounts of smectite. Sufficient additional iron and magnesium are apparently available for the complete transformation of clinoptilolite. Iron is probably present as iron oxides and hydroxides; some of the magnesium may also be present as oxides and hydroxides, although the form of magnesium in the high clinoptilolite rocks is unclear. To the extent that magnesium is present in aluminum silicates, the amount of calcite produced in Eq. (15) will be reduced.

Although Eq. (15) is dependent on $a_{CO_3^{2-}}$ and pH, the process is much more dependent on $a_{SiO_{2(aq)}}$ because of the larger exponent of $a_{SiO_{2(aq)}}$ in (17). Because of the complex interplay of parameters affecting this reaction, more detailed numerical modeling is needed. Smectite generally coexists with clinoptilolite in Yucca Mountain, but appreciable clinoptilolite reaction to form smectite appears to happen only at $a_{SiO_{2(aq)}}$ near cristobalite saturation. Varying $a_{CO_3^{2-}}$ with $a_{SiO_{2(aq)}}$ near cristobalite saturation probably changes the calcium/sodium partitioning between coexisting clinoptilolite and smectite. Equation (17) indicates that at higher $a_{CO_3^{2-}}$ the smectite will become more calcium rich and the clinoptilolite less calcium rich. Equation (18) indicates that the converse will be true for sodium.

The uppermost clinoptilolites in Yucca Mountain tend to be calcium rich. While the rock in which these clinoptilolites occur tends also to be calcium rich, this is not universally true as in UE-25a#1. These clinoptilolites have low potassium contents indicative of $a_{SiO_{2(aq)}}$ near cristobalite saturation. The low $a_{SiO_{2(aq)}}$ is probably caused by equilibration of the water with immediately overlying tridymite- and cristobalite-bearing rocks as the water moves downward. These clinoptilolites generally occur with smectite. The high calcium content probably results from low $a_{CO_3^{2-}}$. Low values of $a_{CO_3^{2-}}$ probably result from limited water movement in the unsaturated zone where these clinoptilolites occur and from the depletion of the limited supply of CO_3^{2-} by the reaction shown in Eq. (15). As Eq. (15) proceeds, H^+ is depleted, reinforcing the effect of CO_3^{2-} depletion. Calcite, predicted as a product of this reaction, has not generally been observed in these rocks, except in USW G-2; however it has been observed in the uppermost clinoptilolite zone of USW G-2. Calcite may not have been observed either because of its tendency to be mobile and form vein fillings or because of low abundance. Equation (15) predicts that

about 0.15 wt% calcite will be formed for every weight percent Ca-smectite. Considering that $x_{\mathrm{Ca-smectite}}$ will probably be less, perhaps considerably less, than 0.5, less than 2 wt% calcite would be expected to result from formation of 30 wt% smectite. A more detailed understanding of this reaction may provide a means of estimating the water flux through this zone.

A similar CO_3^{2-} limited reaction of clinoptilolite to smectite appears to occur in the lower portions of the clinoptilolite zone in USW G-4, UE-25a#1-25b#1h, and J-13 after opal-CT disappears. However, in USW G-1, USW G-2, and USW G-3, $x_{\mathrm{Ca-clinoptilolite}}$ decreases with the appearance of smectite, whereas $x_{\mathrm{Na-clinoptilolite}}$ remains at a high relatively constant value that is probably controlled by equilibrium with analcime. The lower values of $x_{\mathrm{Ca-clinoptilolite}}$ suggest a greater supply of CO_3^{2-} and H^+. With increasing depth, $x_{\mathrm{Ca-clinoptilolite}}$ increases and $x_{\mathrm{Ca-smectite}}$ decreases where smectite and clinoptilolite coexist. This trend probably results from decreasing $a_{SiO_{2(aq)}}$ with depth.

Smectite analyses are available only for USW G-2 and USW G-3. These smectites show a trend of increasing potassium and decreasing sodium and calcium content with increasing depth. This trend, particularly obvious in USW G-2, corresponds to a transition from smectite to illite (Caporuscio et al., 1982). However, the nature of the smectite/illite transition is somewhat uncertain. The smectite/illite transition takes place in pelitic sediments in the temperature range from about 60 to 150°C. However, the extent of conversion of smectite to illite layers can vary even at a given temperature (Perry and Hower, 1972; Bruce 1984). It is not known whether the observed extent of reaction reflects a difference in pressure, pore fluid composition, bulk chemistry of the shale, or composition of the starting smectite or whether it is a time effect reflecting the kinetics of the reaction (Eberl and Hower, 1976; Roberson and Lahann, 1981). The complexity of the problem increases with the uncertainty as to the correct thermodynamic representation for mixed layer smectite/illite. Zen (1962) pointed out that either a solid solution or a two-phase aggregate representation of smectite/illite may be correct. This uncertainty remains unresolved. Aagaard and Helgeson (1983) have used a solid solution model, whereas Garrels (1984), using the same data set, treats the montmorillonite and illite interlayers as separate phases.

It seems likely that aqueous silica activities substantially above quartz saturation are in equilibrium with highly smectitic clays. This conclusion is consistent with both Aagaard and Helgeson (1983) and Garrels (1984). The Garrels' model, treating montmorillonite and illite as separate phases, indicates that at 25°C the transition takes place about midway, on a logarithmic scale, between quartz and amorphous silica saturation. Although the

aqueous silica activity for the transition will increase with increasing temperature, its relationship to the solubility of quartz should remain approximately constant. For the aqueous silica activity to remain high, as indicated by the water composition data compiled by Aagaard and Helgeson (1983), the clay reaction rate must be faster than that for quartz precipitation. The rate of montmorillonite to illite conversion will then be determined by the rate of quartz precipitation. Such a model explains the broad temperature range in which the observed smectite/illite conversion takes place (Hower, 1981; Bruce, 1984) and explains the observed variation of the temperature dependence on time of burial. The model does not explain why the transition stops with approximately 20% smectite layers remaining.

However, if we use the solid solution model (Aagaard and Helgeson, 1983) for smectite/illite, the smectite/illite reaction can proceed at equilibrium as the aqueous silica activity in equilibrium with the clay decreases. The model (Aagaard and Helgeson, 1983) suggests that complete conversion to illite is achieved before quartz saturation is reached. Uncertainties in both the model and the thermodynamic data allow that the smectite/illite reaction stops at 20% montmorillonite layers when it comes into equilibrium with quartz. The conversion rate of montmorillonite to illite layers would still be determined by the rate of quartz precipitation; however, as the aqueous silica activity produced by the clay reaction approached quartz saturation, the quartz precipitation rate would approach zero and the smectite to illite reaction would stop.

Assuming that smectite/illite can be represented by a solid solution of Ca-smectite, Na-smectite, and K-illite endmembers, reactions among the endmembers can be described by

$$\underset{\text{K-feldspar}}{1.9KAlSi_3O_8} + \underset{\text{Ca-smectite}}{Ca_{.55}(Mg,Fe)_{.9}Al_{3.3}Si_{7.8}O_{20}(OH)_4} + 1.1H^+ + 0.55CO_3^{2-}$$

$$\rightarrow \underset{\text{K-illite}}{K_{1.9}(Mg,Fe)_{.9}Al_{4.1}Si_7O_{20}(OH)_4} + \underset{\text{calcite}}{0.55CaCO_3} + \underset{\text{Kaolinite}}{0.28Al_4Si_4O_{10}(OH)_8} + \underset{\text{aqueous silica}}{5.38SiO_2} \qquad (19)$$

and

$$\underset{\text{K-feldspar}}{1.9KAlSi_3O_8} + \underset{\text{Na-smectite}}{Na_{1.1}(Mg,Fe)_{.9}Al_{3.3}Si_{7.8}O_{20}(OH)_4} +$$

$$\rightarrow \underset{\text{K-illite}}{K_{1.9}(Mg,Fe)_{.9}Al_{4.1}Si_7O_{20}(OH)_4}$$

$$+ \underset{\text{analcime}}{1.28Na_{.86}Al_{.86}Si_{2.14}O_6} + \underset{\text{aqueous silica}}{3.76SiO_2} \tag{20}$$

with equilibrium constants

$$K = \frac{a^{5.38}_{SiO_{2(aq)}} x_{K-illite}}{a^{1.1}_{H^+} a^{.55}_{CO_3^{2-}} x_{Ca-smectite}} \tag{21}$$

and

$$K = \frac{a^{3.76}_{SiO_{2(aq)}} x_{K-illite}}{x_{Na-smectite}}. \tag{22}$$

These reactions show that the observed progression of minerals with depth below the clinoptilolite zones can also be explained by decreasing $a_{SiO_{2(aq)}}$. Kaolinite is present and calcite is most abundant in USW G-2 and UE-25b#1h where conversion to illite is nearly complete (Caporuscio et al., 1982). Analcime is generally more abundant at increasing depth, but tends to diminish in the illite zone of USW G-2. This is probably due to the replacement of analcime by albite for which the reaction is

$$\underset{\text{analcime}}{Na_{.86}Al_{.86}Si_{2.14}} + \underset{\text{aqueous silica}}{0.44SiO_2} \rightarrow \underset{\text{albite}}{0.86NaAlSi_3O_8}. \tag{23}$$

The equilibrium constant for this reaction is

$$K = a^{.44}_{SiO_{2(aq)}}, \tag{24}$$

so there should be a particular $a_{SiO_{2(aq)}}$ at which analcime transforms to albite. The exact form of the equilibrium constant and $a_{SiO_{2(aq)}}$ depends on the Al/Si ratio of the analcime. More importantly Eq. (24) predicts that albite should be stable at higher $a_{SiO_{2(aq)}}$ than

analcime, which is contrary to the assumption that $a_{SiO_{2(aq)}}$ decreases with depth in Yucca Mountain. Albite with a high degree of aluminum/silicon ordering (the stable form at low temperature) is probably stable with respect to analcime at $a_{SiO_{2(aq)}}$ intermediate between cristobalite and quartz saturation (Duffy, 1985). However, it appears that the highly ordered form has difficulty crystallizing at low temperature. Albite that is more disordered could form more easily, but is not stable with respect to analcime at low temperature.

The variable $a_{SiO_{2(aq)}}$ in Yucca Mountain appears to account for the mineral transformations that have been observed. Only the stability of mordenite has not been considered. Mordenite stability is difficult to examine because of the limited information on its composition. The limited compositional data available suggest that the equilibria between clinoptilolite and mordenite can be described by the reactions

$$\underset{\text{Na-mordenite}}{Na_{1.8}Al_{1.8}Si_{10.2}} \rightarrow 0.83\underset{\text{Na-clinoptilolite}}{Na_{2.18}Al_{2.18}Si_{9.82}O_{24}} + \underset{\text{aqueous silica}}{2.09SiO_2}, \tag{25}$$

$$\underset{\text{K-mordenite}}{K_{1.8}Al_{1.8}Si_{10.2}} \rightarrow 0.83\underset{\text{K-clinoptilolite}}{K_{2.18}Al_{2.18}Si_{9.82}O_{24}} + \underset{\text{aqueous silica}}{2.09SiO_2}, \tag{26}$$

and

$$\underset{\text{Ca-mordenite}}{Ca_{.9}Al_{1.8}Si_{10.2}} \rightarrow 0.83\underset{\text{Ca-clinoptilolite}}{Ca_{1.09}Al_{2.18}Si_{9.82}O_{24}} + \underset{\text{aqueous silica}}{2.09SiO_2}. \tag{27}$$

The equilibrium constants for these reactions have the general form

$$K = \frac{a_{SiO_{2(aq)}}^{2.09} \, {}^{\nu}X_{\text{clinoptilolite}}}{{}^{\nu}X_{\text{mordenite}}}. \tag{28}$$

Generally, clinoptilolite is probably stable to slightly lower $a_{SiO_{2(aq)}}$ than is mordenite, but this may vary with bulk composition. As noted earlier, mordenite probably contains more sodium than does coexisting clinoptilolite. Because of this, mordenite might remain stable to lower $a_{SiO_{2(aq)}}$ than clinoptilolite if the bulk composition is high in sodium.

VI. REACTION RATES

Both water chemistry and mineral distribution in Yucca Mountain appear to be consistent with the assumptions that the solubility of the most soluble silica polymorph present

in a given location controls $a_{SiO_{2(aq)}}$ and that changing $a_{SiO_{2(aq)}}$ largely controls the observed mineral transitions in Yucca Mountain. The metastable state of silica polymorphs in Yucca Mountain implies that mineral alteration is an ongoing process. However, the rate at which reactions can proceed is limited by the rate of transformation of the silica polymorphs. Several factors such as pressure, pH, and temperature are known to affect the rate of silica polymorph transitions, but only temperature can be quantified at this time. Duffy (1993) describes in detail the kinetic model used here. The model assumes that the transitions from disordered opal-CT to quartz occur in a stepwise manner. Disordered opal-CT transforms to ordered opal-CT, which is nearly equivalent to cristobalite, through a solid state reaction. A decrease in the 101 spacing in the crystal lattice of opal-CT reflects the progress of this reaction. When the 101 spacing reaches 4.05Å, transformation of the ordered opal-CT/cristobalite to quartz begins by means of a dissolution/precipitation reaction. This reaction sequence agrees with the x-ray diffraction data of Bish and Chipera (1986), where little quartz was found coexisting with opal-CT, while considerable quartz was present with cristobalite. Even the small amounts of quartz present with opal-CT may be primary phenocrysts that did not form from opal-CT.

The rate equation for the ordering of opal-CT is

$$\frac{dS}{dt} = -kS, \tag{29}$$

where

$$S = d(101) - 4.040\text{Å}, \tag{30}$$

t is the reaction time and k is the rate constant. The rate equation for the transformation of ordered opal-CT/cristobalite to quartz is

$$\frac{dC_r}{dt} = -k, \tag{31}$$

where C_r is the ratio of cristobalite/(cristobalite + quartz). The dependence of the rate constants on temperature is given by

$$k = Ae^{-E/RT}, \tag{32}$$

where A is the frequency factor, E is the activation energy, R is the gas constant, and T is the temperature in kelvin. The frequency factors and activation energies for Eqs. (29) and (31) are given in Table II.

TABLE II

$A(yr^{-1})$	E(kcal/mol)	Reaction	Reference
$2.62 \cdot 10^7$	20.	Ordering of Opal-CT	Kano (1983)
$1.11 \cdot 10^9$	23.2	Opal-CT/Quartz	Ernst & Calvert (1969)

Duffy (1993) observed that these equations predict disappearance of opal-CT and cristobalite near the depths observed in Yucca Mountain if the present temperature distribution existed throughout the lifetime of the rocks. Based on clay mineralogy, Caporuscio et al. (1982) and Bish and Semarge (1982) suggest temperatures as high as 200°C may have been attained in the past at the bottom of USW G-2. The model that has been presented here does not assume that elevated temperature is necessary for the formation of illite, but does assume that $a_{SiO_{2(aq)}}$ must be below cristobalite saturation, which would require that the only remaining silica polymorph is quartz. Highly illitic clay is present at depth in USW G-2 (Caporuscio et al., 1982) and near the bottom of USW G-1, where only quartz is present. However, illites from 1181 and 1576 m in USW G-2 and 1718 m in USW G-1 have K-Ar dates of 10.9 ± 0.6 m.y. (Broxton et al., 1987) (sample depths provided by David L. Bish, personal communication). This K-Ar date is contemporaneous with the younger eruptions from 11.3 to 9.5 m.y. (Marvin et al., 1970) of the Timber Mountain-Oasis Valley caldera complex located north of Yucca Mountain. Transformation of metastable polymorphs to quartz at 10.9 m.y. may have been caused by a heating event associated with these eruptions.

Fig. 25 shows the model calculation of the evolution of silica polymorphs at 85°C, starting with all of the silica present as disordered opal-CT with a 101 lattice spacing of 4.13Å. I predict the complete conversion to quartz to require about 0.26 m.y., which is in reasonable agreement with the 0.4 m.y. difference in time between the age of the beginning of the ash-flow cycles of the Timber Mountain Tuff and the most probable time for crystallization of the illite. This time span could possibly have been 0 to greater than 1 m.y. Adequate data do not exist to determine a precise temperature history for the drill holes in Yucca Mountain, but two possible temperature histories have been examined. The

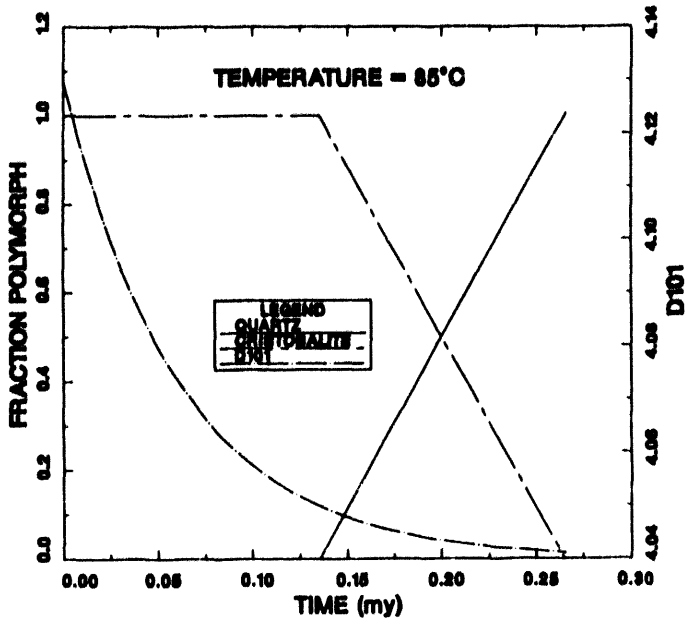

Fig. 25. Model prediction for the evolution of silica polymorphs at 85°C. D101 is the spacing of the 101 planes in the crystal lattice of opal-CT.

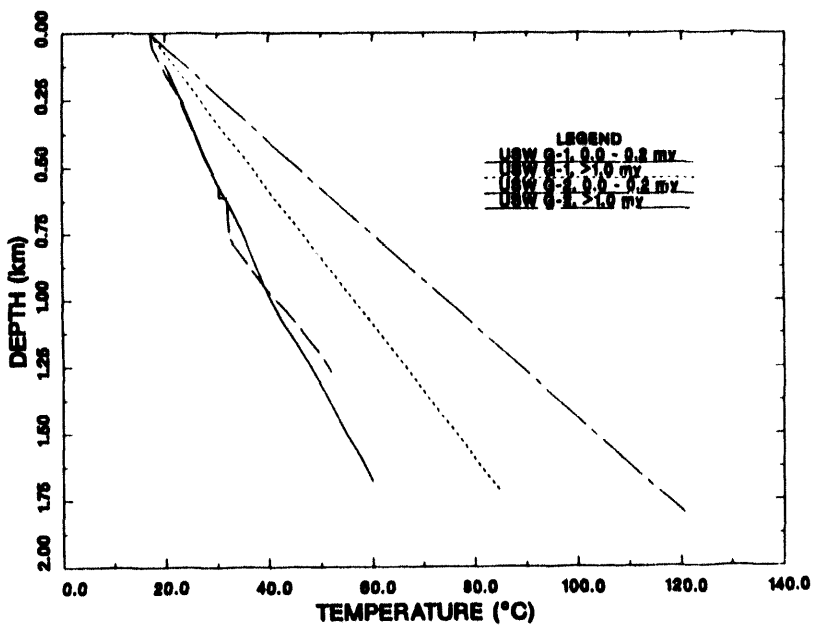

Fig. 26. Model temperature histories for USW G-1 and USW G-2.

first temperature history, illustrated in Fig. 26, shows the present-day temperature profile for USW G-1 (Sass and Lachenbruch, 1982) and for USW G-2 (Sass et al., 1983). I assume that the temperature rose to 85°C at the initial time at the position of the uppermost dated illite, that is at 1181-m depth in USW G-2 and at 1718 m in USW G-1. I assume a linear temperature gradient to the surface, which remains at the current surface temperature. This temperature distribution remains constant for 0.2 m.y. and then decays to the current temperature distribution at 1.0 m.y., and remains at those values.

Fig. 27 models the history at 1718 m, the depth of the dated illite, in USW G-1. The model predicts that all cristobalite/opal-CT will have disappeared at about 0.3 m.y., leaving approximately 0.1 m.y. for the crystallization of illite. These predictions agree with the kinetic data of Eberl and Hower (1976) that predict that the smectite/illite transition takes 0.1 m.y. at 75°C. Therefore, the model provides for the crystallization of illite at the correct time. Figs. 28 and 29 show model calculations for the present depths of cristobalite and opal-CT disappearance respectively. The model does not contain the rate laws for the devitrification of glass forming disordered opal-CT, but assumes that the dominant silica phase is disordered opal-CT at the beginning of the heating event. If we accept this assumption, the model corresponds well to the observed depth of disappearance of cristobalite and opal-CT; it predicts 11 m.y. for the disappearance of opal-CT at 792 m and 12 m.y. for the disappearance of cristobalite at 1104 m, agreeing with the 11.3 m.y. age for the onset of Timber Mountain activity. Similar results are presented in Figs. 30 to 32 for USW G-2. Although opal-CT has not been distinguished from cristobalite in USW G-2, its deepest occurrence has been estimated at 762 m based on the abrupt increase in quartz content. The results for USW G-2 also agree with observation, predicting disappearance of cristobalite at 11.6 m.y. and disappearance of opal-CT at about 12 m.y. Heating probably started slightly earlier with emplacement of magma into a shallow chamber (Christiansen et al., 1977). If heating was caused by magma associated with eruption of the Paintbrush Tuff, it may have commenced as early as 13 m.y. B.P. The model results would be similar except that slightly lower maximum temperature would be required.

I noted earlier that higher temperatures have been inferred from the observed clay assemblages. Other investigators based this inference primarily on observations in pelitic sediments (Perry and Hower, 1970; Hower, 1981; Bruce, 1984). Figs. 33 to 35 show the results of model calculations for a second temperature history for USW G-2 with a maximum temperature of 150°C at 1181 m. These results are as compatible with the observations as the results with a maximum temperature of 85°C. However, the interval

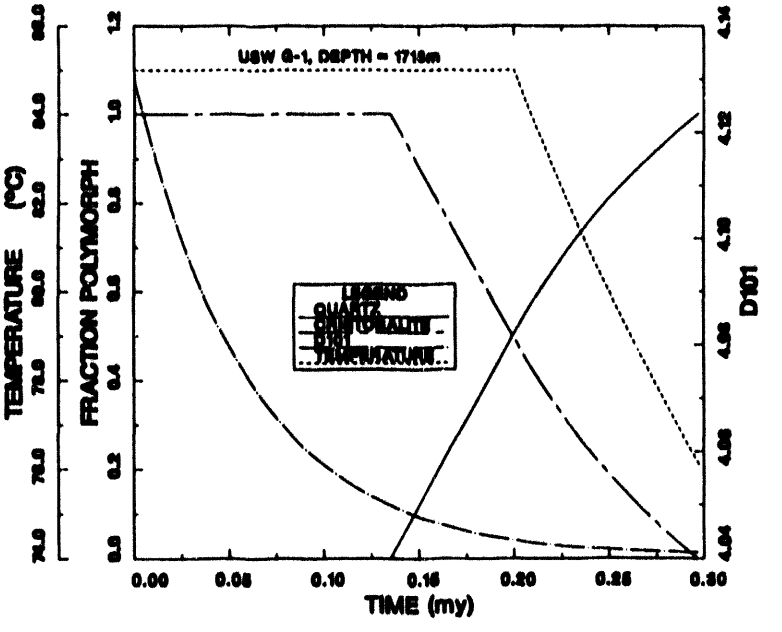

Fig. 27. Model for the evolution of silica polymorphs at 1718 m in USW G-1, assuming a maximum temperature of 85°C was reached at 1718 m.

of maximum temperature lasted only 2 500 years and temperatures returned to current temperatures at 12 500 years after the start of the model. The data from pelitic sediments suggest that smectite to illite conversion should require millions of years even at 150°C. Apparently either the kinetics of smectite-to-illite conversion are considerably faster in Yucca Mountain than in pelitic sediments or thermal gradients have been very nonlinear in the past. One possible explanation for faster kinetics of reaction in Yucca Mountain than in pelitic sediments may be a difference in pH. Most of the pelitic sediments which have been studied are oil shales that, because of a high content of organic acids, may have significantly lower pH than do Yucca Mountain waters.

If the model presented here is correct in that the smectite-to-illite reaction is controlled by $a_{SiO_{2(aq)}}$, the rate of conversion of smectite to illite cannot proceed faster than the rate of crystallization of quartz. The rate of quartz crystallization is highly pH dependent (Duffy, 1993). The distilled water used the by Eberl and Hower (1976) when determining the rate of smectite-to-illite conversion would tend to have produced pH conditions similar to Yucca Mountain water. The rate determined by Eberl and Hower (1976) is compatible with the rate observed in Yucca Mountain. These observations suggest that pH may influence the rate of smectite-to-illite conversion.

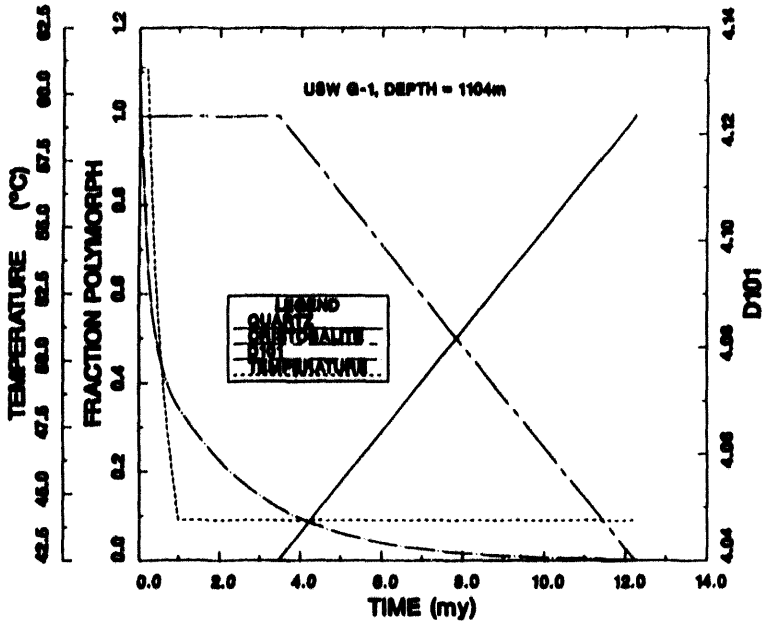

Fig. 28. Model for the evolution of silica polymorphs at 1104 m in USW G-1, assuming a maximum temperature of 85°C was reached at 1718 m.

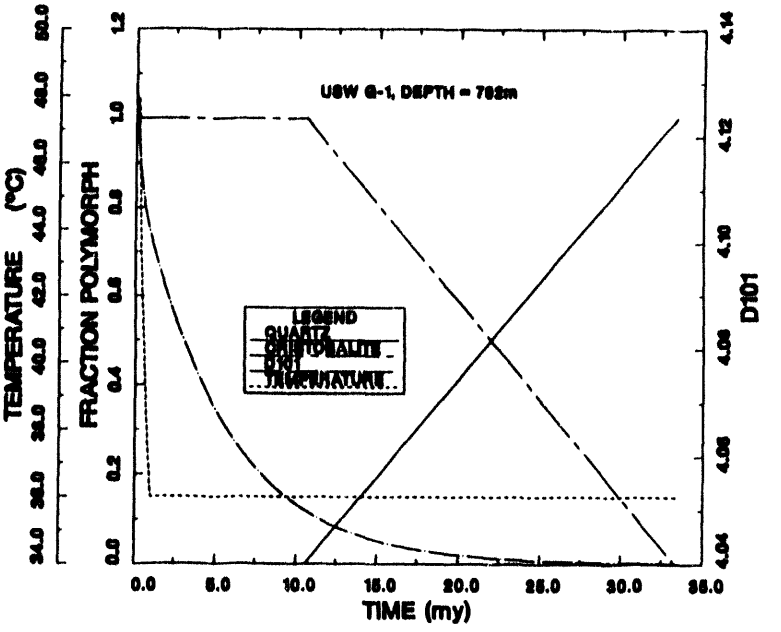

Fig. 29. Model for the evolution of silica polymorphs at 792 m in USW G-1, assuming a maximum temperature of 85°C was reached at 1718 m.

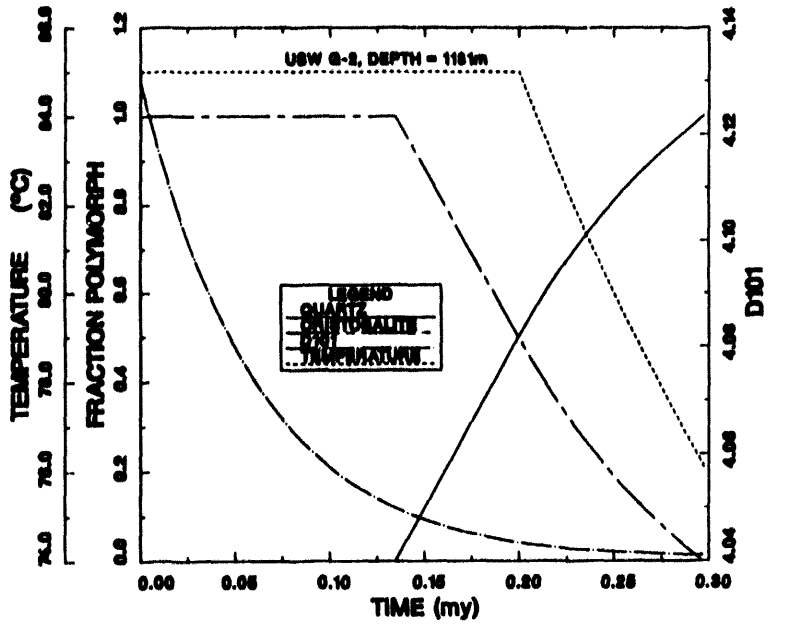

Fig. 30. Model for the evolution of silica polymorphs at 1181 m in USW G-2, assuming a maximum temperature of 85°C was reached at 1181 m.

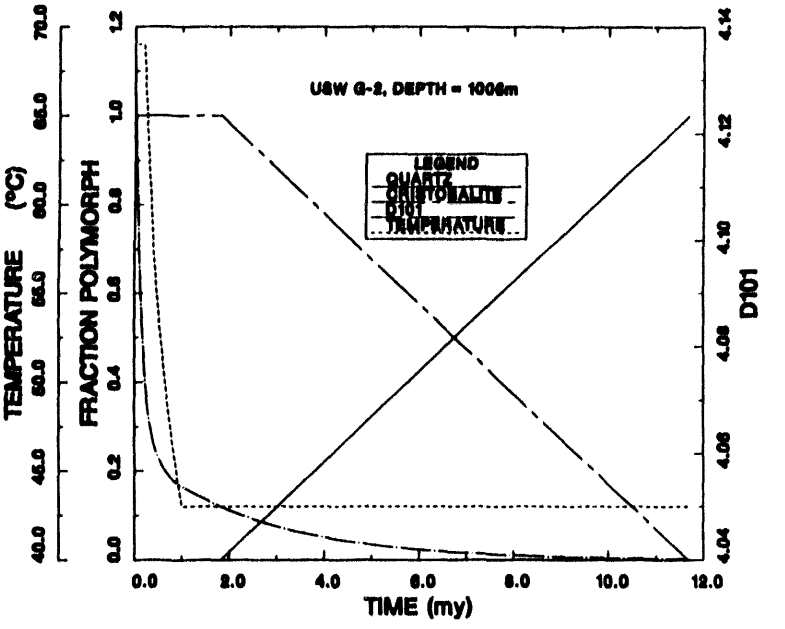

Fig. 31. Model for the evolution of silica polymorphs at 1006 m in USW G-2, assuming a maximum temperature of 85°C was reached at 1181 m.

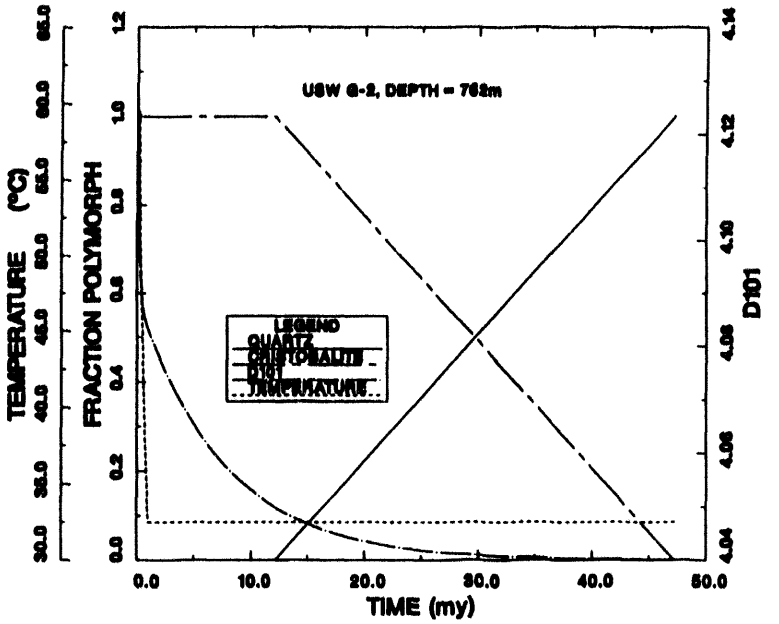

Fig. 32. Model for the evolution of silica polymorphs at 762 m in USW G-2, assuming a maximum temperature of 85°C was reached at 1181 m.

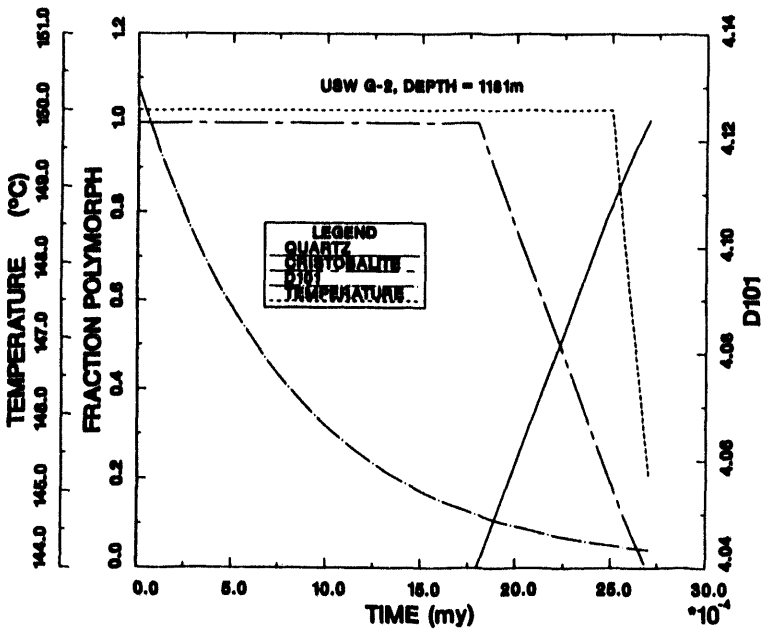

Fig. 33. Model for the evolution of silica polymorphs at 1181 m in USW G-2, assuming a maximum temperature of 150°C was reached at 1181 m.

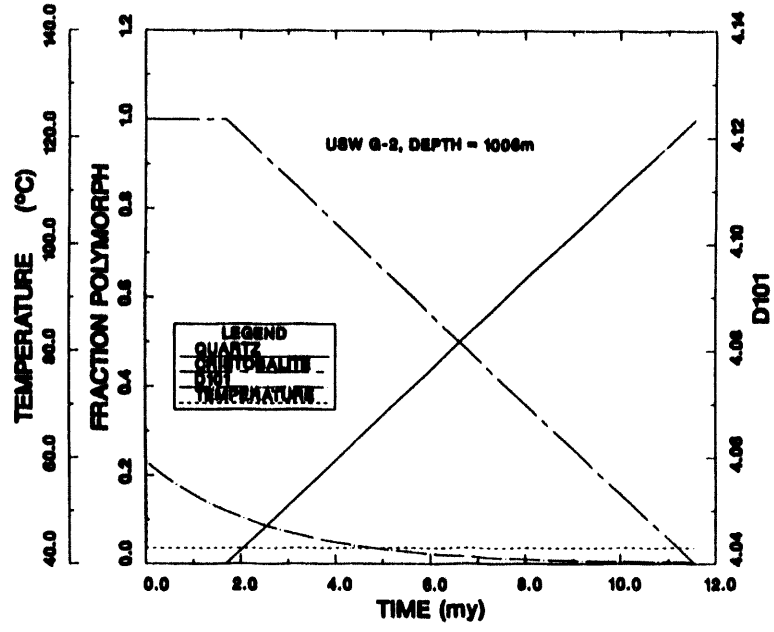

Fig. 34. Model for the evolution of silica polymorphs at 1006 m in USW G-2, assuming a maximum temperature of 150°C was reached at 1181 m.

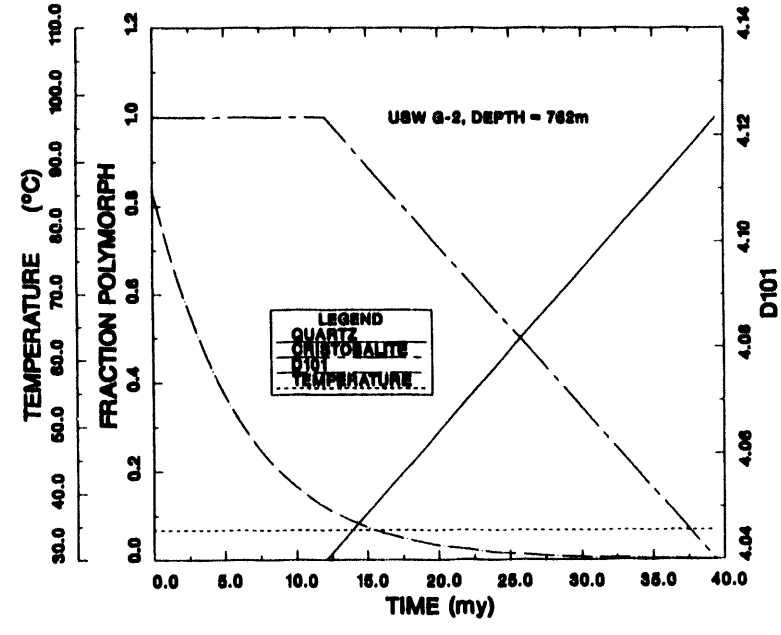

Fig. 35. Model for the evolution of silica polymorphs at 762 m in USW G-2, assuming a maximum temperature of 150°C was reached at 1181 m.

VII. CONCLUSIONS

Mineral alteration in Yucca Mountain is primarily controlled by $a_{SiO_{2(aq)}}$ with $a_{CO_3^{2-}}$ and pH being of secondary importance. To a first approximation, $a_{SiO_{2(aq)}}$ appears to be controlled by the solubility of the most soluble silica polymorph present. Because such reactions as the conversion of K-clinoptilolite to K-feldspar can proceed only as $a_{SiO_{2(aq)}}$ drops, their rates can be constrained by the rate of silica polymorph transformations, if the most soluble silica polymorph controls $a_{SiO_{2(aq)}}$ at its solubility. If this assumption is made, a simple model for the kinetics of silica polymorph evolution provides a good explanation for the present mineral distribution in Yucca Mountain.

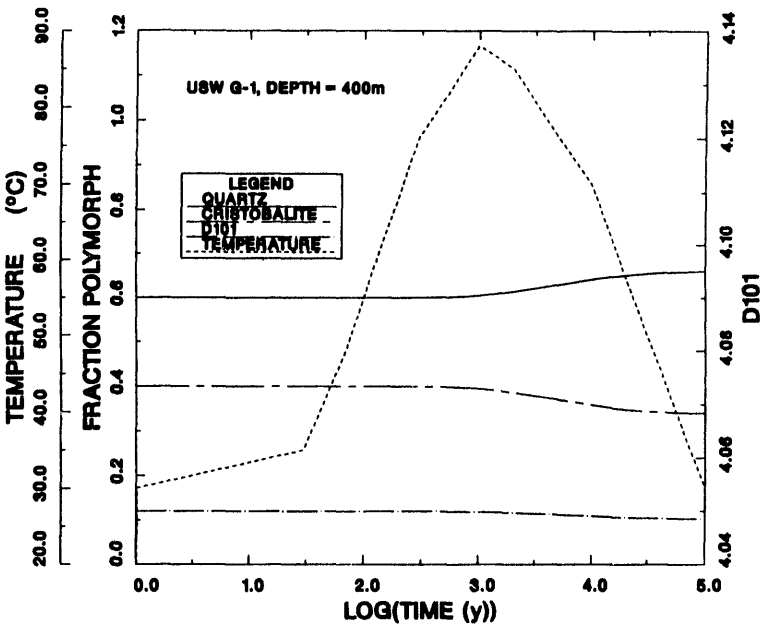

Fig. 36. Predicted future evolution of silica polymorphs at 400 m in USW G-1.

This kinetic model can be used to predict future mineral alteration. Fig. 36 shows the predicted change in the silica polymorphs at 400-m depth in USW G-1. The calculations shown in this figure use the time/temperature predictions of Johnstone et al. (1984) for limiting properties at the 15% boundary below the Topopah Spring repository horizon. I assume the opal-CT/cristobalite at this level to be sufficiently ordered for conversion to quartz to proceed at the present time. I assume 60% of the initial silica polymorph to be quartz with the remaining 40% cristobalite. The model predicts that there will be an increase on the order of 10% in the amount of quartz in 100 000 yr and that significant

cristobalite will remain. Therefore, I predict $a_{SiO_{2(aq)}}$ will remain constant and I expect no mineral alteration except the minor conversion of cristobalite to quartz.

Using the same temperature history as in Fig. 36, Fig. 37 illustrates predicted silica polymorph alteration at 430 m depth. This location was examined because partially disordered opal-CT is present. Although I expect a small amount of ordering of the opal-CT, the fully ordered state will probably not be reached and no quartz precipitation is expected. The $a_{SiO_{2(aq)}}$ will decrease slightly; therefore, some K-clinoptilolite will probably convert to K-feldspar and lesser amounts of sodium or calcium clinoptilolite might convert to smectite. Some mordenite will probably also transform to K-feldspar and smectite. Unless the present opal-CT is already highly ordered, which seems unlikely based on the potassium content of the clinoptilolite in the rock, Na-clinoptilolite is unlikely to transform to analcime. Fig. 38 shows predictions for 644-m depth in USW G-1, which corresponds to 85% boundary below the Topopah Spring repository horizon. I expect minor change in ordering of the opal-CT and quite minor alteration of the type expected at 430 m at this location.

I base these predictions on the assumption that the kinetics of silica polymorph transformation will not be affected by parameters other than temperature. In particular, if emplacement of a repository caused an increase in the pH of the surrounding water, the rates of mineral alteration could be greatly accelerated. Increased $a_{CO_3^{2-}}$ could also cause alteration of calcium-rich clinoptilolite and could promote both conversion of clinoptilolite to smectite and smectite to illite. Smectite alteration in the Topopah Spring Member, although possible, has not been examined in detail. At 150°C, the conversion of the remaining cristobalite to quartz would require only a few hundred years if water is present, which would require fluid pressure of about 5 bar. Once cristobalite disappeared, conversion of smectite to illite would be probable. Such a conversion would probably reduce the sorptive capacity of the rock.

The model suggests that mineral alteration would probably be minor for at least 100 000 yr after emplacement of a repository in Yucca Mountain if the thermal model used here is followed; but it also suggests that mineral reactions are occurring in Yucca Mountain at the present time. Some of these reactions involve H^+ and CO_3^{2-} that must be supplied by the water. Therefore, it may be possible to combine reaction rate data with water composition data to help estimate past water fluxes in Yucca Mountain. These studies could be used to examine the flux of water through the basal vitrophyre of the

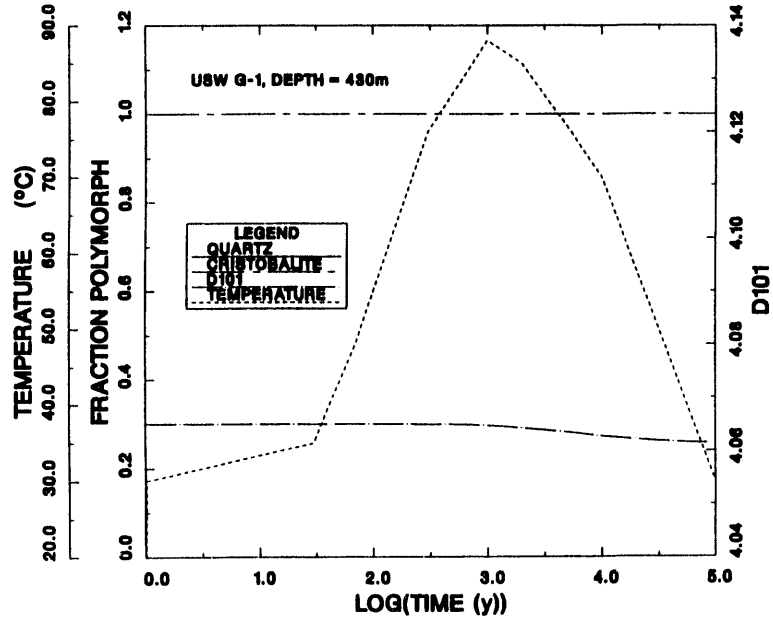

Fig. 37. Predicted future evolution of silica polymorphs at 430 m in USW G-1.

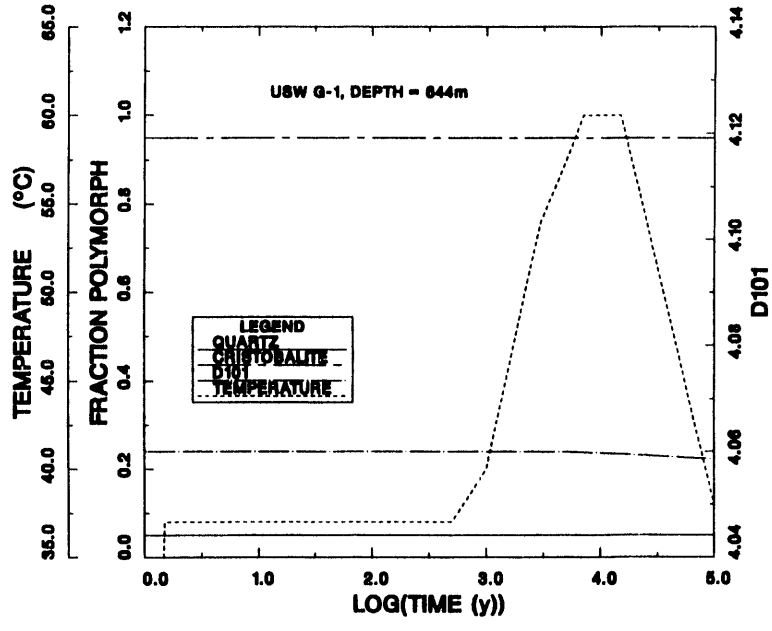

Fig. 38. Predicted future evolution of silica polymorphs at 644 m in USW G-1.

Topopah Spring Member and might be linked to variations in HCO_3^- and pH across Yucca Mountain to help confirm the direction and rate of flow.

VIII. ACKNOWLEDGEMENTS

I have benefited greatly from discussions with David Bish and David Vaniman. I also owe a great deal to the support and encouragement of Bruce Crowe. This work has been supported by the Nevada Nuclear Waste Storage Investigations Project, which is managed by the Waste Management Project Office of the US Department of Energy.

REFERENCES

Aagaard, P. and H. C. Helgeson, "Activity/composition relations among silicates and aqueous solutions: II. chemical and thermodynamic consequences of ideal mixing of atoms on homological sites in montmorillonites, illites, and mixed-layer clays," Clays and Clay Minerals **31**, 207-217 (1983). NNA.891006.0210

Bish, D. L. and R. Ellen Semarge, "Mineralogic variations in a silicic tuff sequence: Evidence for diagenetic and hydrothermal reactions," Nineteenth Circum-Pacific Clay Minerals Society Annual Meeting, Hilo, Hawaii, 1982. NNA.870406.0234

Bish, D. L. and S. J. Chipera, "Mineralogy of drill holes J-13, UE-25A#1, and USW G-1 at Yucca Mountain, Nevada," Los Alamos National Laboratory report LA-10764-MS (September 1986). NNA.890523.0057

Bish, D. L. and D. T. Vaniman, "Mineralogic summary of Yucca Mountain, Nevada," Los Alamos National Laboratory report LA-10543-MS (October 1985). NNA.870407.0330

Broxton, D. E., D. L. Bish, and R. G. Warren, " Distribution and chemistry of diagenetic minerals at Yucca Mountain, Nye County, Nevada," Clays and Clay Minerals **35**, 89-110 (1987). NNA.890222.0053

Broxton, D., D. Vaniman, F. Caporuscio, B. Arney, and G. Heiken, "Detailed petrographic descriptions and microprobe data for drill holes USW-G2 and UE25b-1h, Yucca Mountain, Nevada," Los Alamos National Laboratory report LA-9324-MS (October 1982). NNA.931029.0052

Broxton, D. E., R. G. Warren, R. C. Hagan, and G. Luedemann, "Chemistry of diagenetically altered tuffs at a potential nuclear waste repository, Yucca Mountain, Nye

County, Nevada," Los Alamos National Laboratory report LA-10802-MS (October 1986). NNA.890327.0036

Bruce, C. H., "Smectite dehydration Its relation to structural development and hydrocarbon accumulation in northern Gulf of Mexico Basin," AAPG Bull. **68**, 673-683 (1984). NNA.900508.0011

Caporuscio, F., D. Vaniman, D. Bish, D. Broxton, B. Arney, G. Heiken, F. Byers, R. Gooley, and E. Semarge, "Petrologic studies of drill cores USW-G2 and UE25b-1H, Yucca Mountain, Nevada," Los Alamos National Laboratory report LA-9255-MS (July 1982). NNA.870519.0041

Carlos, B. A., "Minerals in fractures of the unsaturated zone from drill core USW G-4, Yucca Mountain, Nye County, Nevada," Los Alamos National Laboratory report LA-10415-MS (April 1985). NNA.920506.0037

Carlos, B. A., "Minerals in fractures of the saturated zone from drill core USW G-4, Yucca Mountain, Nye County, Nevada," Los Alamos National Laboratory report LA-10927-MS (April 1987). NNA.870708.0026

Christiansen, R. L., P. W. Lipman, W. J. Carr, F. M. Byers Jr., P. P. Orkild, and K. A. Sargent, "Timber Mountain-Oasis Valley caldera complex of southern Nevada," Geological Society of America Bulletin **88**, 943-959 (1977). NNA.870406.0166

Deer, W. A., R. A. Howie, and J. Zussman, *Rock-Forming Minerals. 3. Sheet Silicates*, Longmans, Green and Co. Ltd., London (1962), pp. 164-212. NNA.931029.0043

Dibble W. E., Jr., and W. A. Tiller, " Kinetic model of zeolite paragenesis in tuffaceous sediments," Clays and Clay Minerals **29**, 323-330 (1981). NNA.870406.0093

Duffy, C. J., "Letter report on the thermodynamics of analcime," TWS-INC7-4/85-10 Los Alamos National Laboratory memorandum, (1985). NNA.900709.0172

Duffy, C. J., "Kinetics of silica phase transitions," Los Alamos National Laboratory report LA-12564-MS (July 1993). NNA.900112.0346

Eberl, D. and J. Hower, "Kinetics of illite formation," Geological Society of America Bulletin **87**, 1326-1330 (1976). NNA.931029.0045

Ernst W. G. and S. E. Calvert, "An experimental study of the recrystallization of porcelanite and its bearing on the origin of some bedded cherts," American Journal of Science **267-A**, 114-133 (1969). NNA.900508.0013

Garrels, R. M., "Montmorillonite/illite stability diagrams," Clays and Clay Minerals **32**, 161-166 (1984). NNA.900508.0014

Honda, S. and L. J. P. Muffler, "Hydrothermal alteration in core from research drill hole Y-1, Upper Geyser Basin, Yellowstone National Park, Wyoming," American Mineralogist **55**, 1714-1737 (1970). NNA.931029.0045

Hower, J., "Shale diagenesis," *Short course in clays and the resource geologist*, F. J. Longstaffe, Ed., (Mineralogical Association of Canada, Calgary, 1981), pp. 60-80. NNA.931029.0046

Johnstone, J. K., R. R. Peters, and P. F. Gnirk, "Unit evaluation at Yucca Mountain, Nevada Test Site: Summary report and recommendations," Sandia National Laboratories report SAND83-0372 (June 1984). NNA.870519.0052

Kano, K., "Ordering of opal-CT in diagenesis," Geochemical Journal **17**, 87-93 (1983). NNA.930420.0069

Keith, T. E. C., D. E. White, and M. H. Beeson, "Hydrothermal alteration and self sealing in Y-7 and Y-8 drill holes in northern part of Upper Geyser Basin, Yellowstone National Park, Wyoming," US Geological Survey Professional Paper 1054-A (1978). NNA.931029.0051

Kerrisk, J. F., "Reaction-path calculations of groundwater chemistry and mineral formation at Rainier Mesa, Nevada," Los Alamos National Laboratory report LA-9912-MS (December 1983). NNA.870310.0007

Kerrisk, J. F., "Groundwater chemistry at Yucca Mountain, Nevada, and vicinity," Los Alamos National Laboratory report LA-10929-MS (February 1987). NNA.870507.0017

Levy, S. S., "Petrology of samples from drill holes USW H-3, H-4, and H-5, Yucca Mountain, Nevada," Los Alamos National Laboratory report LA-9706-MS (June 1984). NNA.870519.0048

Marvin, R. F., F. M. Byers, Jr., H. H. Mehnert, P. P. Orkild, and T. W. Stern, " Radiometric ages and stratigraphic sequence of volcanic and plutonic rocks, southern Nye

and western Lincoln Counties, Nevada," Geological Society of America Bulletin **81**, 2657-2676 (1970). NNA.870406.0301

Moiola, R. J., "Authigenic zeolites and K-feldspar in the Esmeralda Formation, Nevada," American Mineralogist **55**, 1681-1691 (1970). NNA.931029.0050

Murata, K. J. and R. R. Larson, "Diagenesis of miocene siliceous shales, Temblor Range, California," Jour. Research. U.S. Geol. Survey **3**, 553-566 (1975). NNA.930420.0075

Perry, E. and J. Hower, "Burial diagenesis of gulf coast pelitic sediments," Clays and Clay Minerals **18**, 165-177 (1970). NNA.900508.0026

Perry, E. A., Jr. and J. Hower, "Late stage dehydration in deeply buried pelitic sediments," AAPG Bull. **56**, 2013-2021 (1972). NNA.931029.0049

Roberson, H. E. and R. W. Lahann, "Smectite to illite conversion rates: Effects of solution chemistry," Clays and Clay Minerals **29**, 129-135 (1981). NNA.931029.0048

Sass, J. H., and A. H. Lachenbruch, "Preliminary interpretation of thermal data from the Nevada Test Site," US Geological Survey Open File Report 82-973 (1982). NNA.870406.0040

Sass, J., A. Lachenbruch, F. Grubb, and T. Moses, "Status of thermal observations at Yucca Mountain, Nevada," US Geological Survey Letter Report (April 1983). NNA.931029.0047

Smyth, J. R., " Zeolite stability constraints on radioactive waste isolation in zeolite-bearing volcanic rocks," Journal of Geology **90**, 195-201 (1982). NNA.870406.0187

Vaniman, D., D. Bish, D. Broxton, F. Byers, G. Heiken, B. Carlos, E. Semarge, F. Caporuscio, and R. Gooley, "Variations in authigenic mineralogy and sorptive zeolite abundance at Yucca Mountain, Nevada, based on studies of drill cores USW GU-3 and G-3," Los Alamos National Laboratory report LA-9707-MS (June 1984). NNA.870519.0043

Walther, J. V. and H. C. Helgeson, "Calculations of the thermodynamic properties of aqueous silica and the solubility of quartz and its polymorphs at high pressures and temperatures," American Journal of Science **277**, 1315-1351 (1977). NNA.921124.0013

Zen, E., "Problem of the thermodynamic status of the mixed-layer minerals," Geochimica et Cosmochimica Acta **26**, 1055-1067 (1962). NNA.900508.0032

DATE
FILMED
1/12/94
END